

**Effects of Crystal Structure and the On-Site Coulomb  
Interactions on the Electronic and Magnetic Structure of  
Pyrochlores  $A_2\text{Mo}_2\text{O}_7$  ( $A= \text{Y}, \text{Gd}, \text{and Nd}$ )**

I. V. Solovyev\*

*Tokura Spin Superstructure Project,*

*ERATO Japan Science and Technology Corporation,*

*c/o National Institute of Advanced Industrial Science and Technology,*

*Central 4, 1-1-1 Higashi, Tsukuba, Ibaraki 305-8562, Japan*

(Dated: October 29, 2018)

## Abstract

Being motivated by recent experimental studies, we investigate magnetic structures of the Mo pyrochlores  $A_2\text{Mo}_2\text{O}_7$  ( $A = \text{Y, Nd, and Gd}$ ) and their impact on the electronic properties. The latter are closely related with the behavior of twelve  $\text{Mo}(t_{2g})$  bands, located near the Fermi level and well separated from the rest of the spectrum. We use a mean-field Hartree-Fock approach, which combines fine details of the electronic structure for these bands, extracted from the conventional calculations in the local-density approximation, the spin-orbit interaction, and the on-site Coulomb interactions amongst the  $\text{Mo}(4d)$  electrons, treated in the most general rotationally invariant form. The Coulomb repulsion  $U$  plays a very important role in the problem, and the semi-empirical value  $U \sim 1.5\text{-}2.5$  eV accounts simultaneously for the metal-insulator (M-I) transition, the ferromagnetic (FM) - spin-glass (SG) transition, and for the observed enhancement of the anomalous Hall effect (AHE). The M-I transition is mainly controlled by  $U$ . The magnetic structure at the metallic side is nearly collinear FM, due to the double exchange mechanism. The transition into the insulating state is accompanied by the large canting of spin and orbital magnetic moments. The sign of exchange interactions in the insulating state is controlled by the Mo-Mo distances. Smaller distances favor the antiferromagnetic coupling, which precludes the SG behavior in the frustrated pyrochlore lattice. Large AHE is expected in the nearly collinear FM state, near the point of M-I transition, and is related with the unquenched orbital magnetization at the Mo sites. We also predict large magneto-optical effect in the same FM compounds.

PACS numbers: 71.70.Gm, 75.25.+z, 71.30.+h, 78.20.Ls

## I. INTRODUCTION

The pyrochlores with the chemical formula  $A_2\text{Mo}_2\text{O}_7$  ( $A$  being the divalent element) exhibit a number of interesting and not completely understood phenomena,<sup>1</sup> which present the main motivation for the analysis of electronic and magnetic structure of these compounds, which we undertake in this work.

- The pyrochlores  $A_2\text{Mo}_2\text{O}_7$  have rather puzzling magnetic phase diagram as a function of averaged ionic radius of  $A$ -sites,  $\langle r_A \rangle$  (Fig. 1).<sup>2,3,4,5</sup> Large  $\langle r_A \rangle$  ( $> R_c \sim 1.047$ ) stabilizes the ferromagnetic (FM) ground state. Typical examples of the FM pyrochlores are  $\text{Nd}_2\text{Mo}_2\text{O}_7$  and  $\text{Gd}_2\text{Mo}_2\text{O}_7$ . The Curie temperature ( $T_C$ ) is of the order of 80 K and slowly increases with  $\langle r_A \rangle$ . Smaller  $\langle r_A \rangle$  ( $< R_c$ ) give rise to the spin-glass (SG) behavior. The characteristic transition temperature into the SG state is of the order of 20 K. The canonical example of the SG compounds is  $\text{Y}_2\text{Mo}_2\text{O}_7$ .<sup>6,7</sup> Now it is commonly accepted that the exchange coupling between nearest-neighbor ( $nn$ ) Mo spins changes the sign around  $R_c$  and becomes antiferromagnetic (AFM) in the SG region. The pyrochlores with AFM interactions in the lattice present a typical example of geometrically frustrated systems with infinitely degenerate magnetic ground state.<sup>8</sup> According to the recent experimental data,<sup>9,10</sup> the SG behavior itself is caused by the combination of the geometrical frustrations and the disorder of the local lattice distortions. The latter is required in order to produce an inhomogeneity in the distribution of the  $nn$  interactions and freeze the random spin configuration. The origin of this behavior itself is very complicated, and we will not be able to address it properly in our work. However, our main concern will be in some sense more general: we will try to understand which parameter of the crystal structure controls the sign of the  $nn$  magnetic interactions, and which part of the electronic structure is responsible for the FM and AFM interactions in these compounds? Contrary to the widespread point of view that the magnetic ground state is controlled by the Mo-O-Mo angle, we will argue that the key parameter is in fact the Mo-Mo distance, which is directly related with the unit cell volume and controls the strength of direct interactions between extended Mo( $4d$ ) orbitals.

According to the experimental data, all Mo pyrochlores which show the SG behavior are small-gap insulators. However, an opposite statement is generally incorrect and in different compounds the ferromagnetism is known to coexist with the metallic as well as insulating behavior.<sup>5</sup> We will show that this trend can be naturally understood in terms of the Mo-

Mo distances and the strength of the on-site Coulomb interaction  $U$  amongst the Mo(4d) electrons.

- The spin-orbit interaction (SOI) in the pyrochlore lattice should generally lead to a non-collinear magnetic ordering associated with the modulation of single-ion anisotropy axes.<sup>11</sup> The magnitude and the main source of this non-collinearity (whether it is primarily associated with the Mo or  $A$  sublattices, and whether it reflects the ordering of spin or orbital magnetic moments) is largely unresolved problem. In the present work we will try to rationalize this question by focusing on the magnetic structure of the Mo sublattice. We will show that as long as the system is metallic (that by itself depends on the strength of the Coulomb interaction  $U$ ), the non-collinearity is very small. However, the transition into the insulating state is accompanied by the abrupt change of the spin and orbital magnetic structures, which become essentially non-collinear.

- Some ferromagnetic (or nearly ferromagnetic) pyrochlores exhibit rather unusual anomalous Hall effect (AHE). A non-vanishing Hall conductivity ( $\sigma_H$ ) emerges near  $T_C$ , then monotonously increases with the decrease of the temperature  $T$ , and reaches the maximal value ( $\sigma_H \sim 20 \text{ } \Omega^{-1} \text{cm}^{-1}$  for  $\text{Nd}_2\text{Mo}_2\text{O}_7$ ) near  $T=0$ . Both magnitude and the temperature dependence of the AHE is in a drastic contrast with other oxide materials, such as colossal-magnetoresistive manganites, for example.<sup>12</sup>

The theory of the AHE (originally called as the extraordinary Hall effect) has very long and rather controversial history.<sup>13,14</sup> Many controversies were related with the lack of the general transport theory and partly – with the lack of good computer facilities in 1950s and 1960s, so that many discussions went around very simplified and not always justified approximations, such as the free-electron and weak scattering limit, the single-orbital tight-binding approach, the classical Boltzmann transport equation, etc.<sup>15</sup> The modern way to address the problem is to use the Kubo formalism and relate  $\sigma_H$  with the real part of the antisymmetric off-diagonal element of the conductivity tensor.<sup>16</sup> From this point of view there are no rigid constraints which would forbid the existence of  $\sigma_H$ , even for periodic systems, once the time-reversal symmetry is violated macroscopically.<sup>17</sup>

The main question is which mechanism leads to the finite value of  $\sigma_H$ . The first one was proposed by Karplus and Luttinger,<sup>13</sup> who stressed the importance of SOI in the problem. Although the concrete scenario considered by Karplus and Luttinger was not correct,<sup>15</sup> they were certainly right by arguing that the SOI is essential in order to couple the spin

polarization of the conduction electrons to the lattice and produce the right-left asymmetry of the stationary Bloch states, which may lead to the Hall current, perpendicular to both the electric field and the magnetization.

However, an exceptionally large  $\sigma_H$  observed in the pyrochlore compounds urged several authors to search for a new and unconventional mechanism for the AHE. Such mechanism was proposed to be due to the spin chirality (basically, the solid angle subtended by three non-coplanar spins) in essentially non-collinear magnetic structure.<sup>1,18</sup> The chirality acts as an effective field, which in the combination with the peculiar lattice geometry is believed to yield a finite  $\sigma_H$ . Although the mechanism itself is rather exotic and there is a great deal of cancellations between different elements of the non-collinear spin structure,<sup>19</sup> these authors were certainly right by stressing the crucial role of the inter-band transitions in the problem of AHE.

In this work we will go back to a more conventional picture and argue that the large value of  $\sigma_H$  in some Mo pyrochlores can be explained by rather unique combination of three factors: (i) large SOI associated with the Mo( $4d$ ) states in the nearly collinear FM structure; (ii) strong enhancement of the SOI by the on-site Coulomb interactions in the  $t_{2g}$  electron systems,<sup>20</sup> and (iii) half-metallic electronic structure of the FM pyrochlores.<sup>21</sup>

Regarding the Coulomb interaction itself, which in our work will be treated as a parameter, we will be able to present a very consistent picture by arguing that  $U \sim 1.5-2.5$  eV in Mo pyrochlores accounts simultaneously for (i) metal-insulator transition; (ii) FM-SG transition; (iii) required enhancement for the AHE in the FM pyrochlore compounds.

The rest of the paper is organized as follows. In Sec. II we remind the basic details of the crystal and electronic structure of  $A_2\text{Mo}_2\text{O}_7$ . We consider three characteristic compounds corresponding to  $A = \text{Y, Gd and Nd}$ . In Sec. III we describe the model Hartree-Fock (HF) approach, which combines the ideas of *ab-initio* electronic structure calculations with the physics of degenerate Hubbard model on the pyrochlore lattice. Secs. IV and V summarize results of calculations without SOI (correspondingly, the basic changes of the electronic structure and the orbital ordering, and the behavior of inter-atomic magnetic interactions). Secs. VI and VII are devoted to the analysis of SOI related properties (the non-collinear magnetic structure, the Hall conductivity, and the magneto-optical effect). Finally, in Sec. VIII we discuss some subtle points related with the interpretation of experimental data and give the summary of the entire work.

## II. MAIN DETAILS OF CRYSTAL AND ELECTRONIC STRUCTURE

The pyrochlores  $A_2\text{Mo}_2\text{O}_7$  crystallize in a face-centered cubic structure with the space group  $Fm\bar{3}d$ , in which  $A$  and Mo occupy correspondingly  $16d$  and  $16c$  positions, and form interpenetrating sublattices of the corner-sharing tetrahedra. There are two non-equivalent types of oxygen sites, and only one internal parameter which may control the properties of  $A_2\text{Mo}_2\text{O}_7$ . That is the coordinate  $u$  of the O  $48f$  sites.

The single Mo tetrahedron is shown in Fig. 2. Four Mo sites are located at  $\boldsymbol{\tau}_1=(0, 0, 0)$ ,  $\boldsymbol{\tau}_2=(0, \frac{1}{4}, \frac{1}{4})$ ,  $\boldsymbol{\tau}_3=(\frac{1}{4}, 0, \frac{1}{4})$ , and  $\boldsymbol{\tau}_4=(\frac{1}{4}, \frac{1}{4}, 0)$ , in units of cubic lattice parameter  $a$ . Each Mo site has sixfold O  $48f$  coordination. The oxygen atoms specify the local coordinate frame around each Mo site. Around the site 1, it is given by

$$\mathbb{R}_1^{\alpha\beta} = \frac{1 + (1 - 8u)\delta_{\alpha\beta}}{\sqrt{64u^2 - 32u + 6}}, \quad (1)$$

where  $\alpha, \beta = x, y, \text{ or } z$ .  $u = \frac{5}{16}$  corresponds to the perfect octahedral environment. In this case  $\widehat{\mathbb{R}}_1 = \|\mathbb{R}_1^{\alpha\beta}\|$  is the standard  $60^\circ$  rotation around the cubic  $[1, 1, 1]$  axis.  $u > \frac{5}{16}$  gives rise to an additional trigonal contraction of the local coordinate frame. Similar matrices associated with the sites 2, 3, and 4 can be obtained by the  $180^\circ$  rotations of  $\widehat{\mathbb{R}}_1$  around  $x, y, \text{ and } z$ , respectively.

Structural parameters of  $A_2\text{Mo}_2\text{O}_7$  are listed in Table I. Corresponding densities of states, obtained in the local-spin-density approximation (LSDA) are shown in Figs. 3 and 4.

In the local coordinate frame, the Mo( $4d$ ) orbitals are split into the triply-degenerate  $t_{2g}$  and doubly-degenerate  $e_g$  states. The splitting is of the order of 4 eV. Twelve  $t_{2g}$  bands are located near the Fermi level and well separated from the rest of the spectrum, which consists of the broad O( $2p$ ) band spreading from -8.5 to -2.5 eV and either Y( $4d$ ) or Gd/Nd( $5d$ ) bands located just above the group of the  $t_{2g}$  states. The Mo( $e_g$ ) states are located in the higher part of the spectrum. Interestingly enough that all three compounds are ferromagnetic, even in the LSDA, that is rather unusual for the  $4d$  oxides, perhaps except the well know example of SrRuO<sub>3</sub>.<sup>24</sup>

The trigonal distortion and different hybridization with the O( $2p$ ) states will further split the Mo( $t_{2g}$ ) states into the one-dimensional  $a_{1g}$  and two-dimensional  $e'_g$  representation.<sup>25</sup>

The crystal structure affects the Mo( $t_{2g}$ ) bandwidth via two mechanisms (see Table I).

1. The Mo-O-Mo angle, which decreases in the direction Nd→Gd→Y. Therefore, the in-

teractions between Mo( $t_{2g}$ ) orbitals which are mediated by the O( $2p$ ) states will also decrease. This effect is partly compensated by the decrease of the Mo-O bondlength for  $A = \text{Gd}$  and  $\text{Y}$ .

2. The lattice parameter  $a$  and the Mo-Mo distance, which decrease in the direction  $\text{Nd} \rightarrow \text{Gd} \rightarrow \text{Y}$  by 2.6%. This will increase direct interactions between extended Mo( $4d$ ) orbitals.

Generally, these two effects act in the opposite directions and partly compensate each other. For example, the width of the  $e'_g$  band is practically the same for all three compounds (Fig. 4). On the other hand, the  $a_{1g}$  orbitals, whose lobes are the most distant from all neighboring oxygen sites are mainly affected by the second mechanism, and the  $a_{1g}$  bandwidth will *increase* in the direction  $\text{Nd} \rightarrow \text{Gd} \rightarrow \text{Y}$ . As we will show in Sec. V, this effect plays a crucial role in the stabilization of AFM interactions in  $\text{Y}_2\text{Mo}_2\text{O}_7$ , which precludes the SG behavior.

Thus, despite an apparent complexity of the crystal structure, the pyrochlores  $A_2\text{Mo}_2\text{O}_7$  present rather simple example of the electronic structure and in order to understand the nature of fascinating electronic and magnetic properties of these compounds, we need to concentrate on the behavior of twelve well isolated Mo( $t_{2g}$ ) bands.<sup>26</sup>

### III. MODEL HARTREE-FOCK APPROACH

In this and subsequent sections we will further elaborate this picture, by cutting the Mo( $t_{2g}$ ) bands from the rest of the spectrum, including the on-site Coulomb interactions amongst the Mo( $4d$ ) electrons, and solving this problem on the level of HF approximation. Hence, our model Hamiltonian has the following form, in the basis of non-relativistic LDA eigenfunctions  $|n\mathbf{k}\rangle$  (LDA is the spin-restricted version of LSDA):

$$\mathcal{H}_{nn'}(\mathbf{k}) = \varepsilon_{n\mathbf{k}}\delta_{nn'} + \mathcal{H}_{nn'}^{SOI}(\mathbf{k}) + \mathcal{H}_{nn'}^U(\mathbf{k}). \quad (2)$$

The spin indices are already included to  $n$  and  $n'$ , which are running from 1 to  $12 \times 2$ . The first term in  $\mathcal{H}_{nn'}(\mathbf{k})$  is the non-magnetic LDA part and  $\varepsilon_{n\mathbf{k}}$  are the LDA eigenvalues.  $\mathcal{H}_{nn'}^{SOI}(\mathbf{k})$  is the matrix of relativistic SOI, which is computed in the conventional way,  $\mathcal{H}_{nn'}^{SOI}(\mathbf{k}) = \langle n\mathbf{k} | \frac{1}{2}\xi(\mathbf{r})(\mathbf{L}, \boldsymbol{\sigma}) | n'\mathbf{k} \rangle$ , where  $\xi(\mathbf{r}) = \frac{1}{c^2} \frac{dV(\mathbf{r})}{dr}$ ,  $\mathbf{L}$  is the operator of angular momentum,  $\boldsymbol{\sigma}$  is the vector of Pauli matrices,  $V(\mathbf{r})$  is the self-consistent LDA potential, and  $c$  is the

velocity of light ( $c \approx 274$  in Ry units). The inclusion of  $\mathcal{H}_{nn'}^{SOI}(\mathbf{k})$  into the model Hamiltonian is optional, that will be always specified in the text.

All magnetic effects are caused by the on-site Coulomb interactions,  $\mathcal{H}_{nn'}^U(\mathbf{k})$ , which can be written in terms of projections onto an orthonormal set of atomic-like Mo( $4d$ ) orbitals  $|\mathbf{R}\tau\mu\rangle$ :

$$\mathcal{H}_{nn'}^U(\mathbf{k}) = \sum_{\mathbf{R}\tau} \sum_{\mu_1\mu_2} \langle n\mathbf{k}|\mathbf{R}\tau\mu_1\rangle \mathcal{U}_{\tau}^{\mu_1\mu_2} \langle \mathbf{R}\tau\mu_2|n'\mathbf{k}\rangle.$$

where  $\mathbf{R}$  are the translation vectors in the face-centered cubic pyrochlore lattice, and  $\tau$  specify different Mo sites in the unit cell.  $\mu \equiv \{s, m\}$  are the joint indices including the spin ( $s = \uparrow$  or  $\downarrow$ ) and orbital ( $m = xy, yz, 3z^2 - r^2, zx, \text{ or } x^2 - y^2$ ) degrees of freedom. Matrix elements of the HF potential,  $\mathcal{U}_{\tau}^{\mu_1\mu_2}$ , can be expressed in the most general rotationally-invariant form as:<sup>20</sup>

$$\mathcal{U}_{\tau}^{\mu_1\mu_2} = \sum_{\mu_3\mu_4} (U_{\mu_1\mu_3\mu_2\mu_4} - U_{\mu_1\mu_3\mu_4\mu_2}) n_{\tau}^{\mu_3\mu_4}, \quad (3)$$

where  $U_{\mu_1\mu_3\mu_2\mu_4} = \langle m_1 m_3 | \frac{1}{r_{12}} | m_2 m_4 \rangle \delta_{s_1 s_2} \delta_{s_3 s_4}$  are the matrix elements of the Coulomb interactions. The latter are fully specified by three radial Slater integrals:  $F^0$ ,  $F^2$ , and  $F^4$ , which are assumed to be *renormalized* from the bare atomic values. Equivalently, one can introduce parameters of the averaged Coulomb interaction,  $U = F^0$ , the intra-atomic exchange coupling,  $J = \frac{1}{14}(F^2 + F^4)$ , and the non-sphericity of the Coulomb interactions between orbitals with the same spin,  $B = \frac{1}{441}(9F^2 - 5F^4)$ . Generally, both  $U_{\text{eff}} = U - J$  and  $B$  contribute to the orbital polarization in solids and affect the properties caused by violation of the time-inversion symmetry.<sup>20</sup>

The density matrix  $\hat{n}_{\tau} \equiv \|n_{\tau}^{\mu\mu'}\|$  can be obtained from the Green function  $\hat{\mathcal{G}}_{\tau\tau'} \equiv \|G_{\tau\tau'}^{\mu\mu'}\|$ , using the standard relation

$$\hat{n}_{\tau} = -\frac{1}{\pi} \text{Im} \int_{-\infty}^{\varepsilon_F} d\varepsilon \hat{\mathcal{G}}_{\tau\tau}(\varepsilon), \quad (4)$$

where

$$G_{\tau\tau'}^{\mu\mu'}(\varepsilon) = \sum_n \frac{1}{\Omega_{\text{BZ}}} \int d\mathbf{k} \frac{\langle \mathbf{R}\tau\mu | \tilde{n}\mathbf{k} \rangle \langle \tilde{n}\mathbf{k} | \mathbf{R}\tau'\mu' \rangle}{\varepsilon - \tilde{\varepsilon}_{n\mathbf{k}} + i\delta} \quad (5)$$

is the spectral representation for the Green function in terms of the eigenfunctions  $|\tilde{n}\mathbf{k}\rangle$  and the eigenvalues  $\tilde{\varepsilon}_{n\mathbf{k}}$  of the Hamiltonian (2).  $\Omega_{\text{BZ}}$  is the volume of the first Brillouin zone.

Eqs. (2), (4) and (5) are solved self-consistently. Then, the total energy is given by

$$E = \sum_n \frac{1}{\Omega_{\text{BZ}}} \int d\mathbf{k} \tilde{\varepsilon}_{n\mathbf{k}} \Theta(\varepsilon_F - \tilde{\varepsilon}_{n\mathbf{k}}) - \frac{1}{2} \sum_{\tau} \sum_{\mu_1\mu_2} \mathcal{U}_{\tau}^{\mu_1\mu_2} n_{\tau}^{\mu_1\mu_2}.$$



According to the constraint-LSDA calculations,<sup>27</sup>  $J$  for Mo is of the order of 0.5 eV, and is not sensitive to details of the crystal environment in solids.  $B$  can be estimated from  $J$  using the ratio  $F^4/F^2 \simeq 0.63$ , which holds for the Slater integrals in the atomic limit. This yields  $B \simeq 0.06$  eV. The Coulomb  $U$  is treated as the parameter in order to consider different scenarios, covering both metallic and insulating behavior of  $A_2\text{Mo}_2\text{O}_7$ . The constraint-LSDA calculations for Mo compounds typically yield  $U \approx 3.0$  eV.<sup>27</sup> This value can be further reduced by allowing for the (proper)  $e_g$  electrons to participate in the screening of the on-site Coulomb interactions between  $t_{2g}$  electrons.<sup>28</sup>

For the practical calculations along this line, it is convenient to use a short atomic-like basis set. For these purposes,  $\varepsilon_{n\mathbf{k}}$  and  $|n\mathbf{k}\rangle$  have been first calculated using the nearly-orthogonal version of the linearized-muffin-tin orbital method in the atomic-spheres approximation (ASA-LMTO).<sup>29</sup> The atomic orbitals  $|\mathbf{R}\tau\mu\rangle$  have been identified with the basis orbitals of the LMTO method. Atomic spheres radii have been chosen so to reproduce the electronic structure obtained by more accurate FLAPW method,<sup>30,31,32</sup> especially for  $t_{2g}$  bands located near the Fermi level. We have also added a number of empty spheres at the  $8a$  and  $32e$  positions of the  $Fd\bar{3}m$  lattice. All calculations have been performed on the mesh of  $12 \times 12 \times 12$   $\mathbf{k}$ -points in the first Brillouin zone.

Formally, our approach is similar to the rotationally-invariant LDA+ $U$ ,<sup>20</sup> except that we apply it only to a limited number of bands, directly responsible for the properties of  $A_2\text{Mo}_2\text{O}_7$  compounds. This will certainly simplify the calculations. In addition, we get rid of several artifacts of the conventional LDA+ $U$  method, such as the subtraction of the double-counting terms, which is a very ambiguous procedure by itself, and in the number of cases leads to a systematic error.<sup>33</sup>

#### IV. CHANGES OF THE ELECTRONIC STRUCTURE CAUSED BY THE ON-SITE COULOMB INTERACTIONS

Let us first discuss results without SOI, assuming FM ordering of the Mo spins. According to the LSDA calculations (Fig. 4), the majority ( $\uparrow$ ) spin  $a_{1g}$  band is fully occupied and the Fermi level crosses the doubly-degenerate  $e'_g$  band. Therefore, it is clear that at some point the Coulomb  $U$  will split the  $e'_g$  band and form an insulating solution with the spontaneously broken  $Fm\bar{3}d$  symmetry. Such situation occurs between  $U = 2.0$  and  $2.5$  eV for all considered

compounds (Fig. 5, the AFM alignment of the Mo spins may open the band gap even for smaller  $U$ , that well correlates with the fact that all SG compounds are insulators).

In the metallic regime realized for small  $U$ , the densities of states are similar to those in LSDA (Figs. 3 and 4), and we will not show them here again. We only mention that the major effect of  $U$  is the shift of the  $\uparrow$ -spin  $a_{1g}$  band to the low-energy part of the spectrum relative to the  $e'_g$  band. Corresponding orbital ordering (the distribution of Mo(4d) electron densities) is shown in Fig. 6. It comes exclusively from the local trigonal distortions of the oxygen octahedra and represents the alternating  $a_{1g}$  orbital densities in the background of degenerate  $e'_g$  orbitals.

Typical densities of states in the insulating phase are shown in Fig. 7. The  $a_{1g}$  band has characteristic for pyrochlores three-peak structure.<sup>35</sup> Smaller band gap in the case of  $Y_2Mo_2O_7$  (Fig. 5) is related with broad minority ( $\downarrow$ ) spin  $a_{1g}$  band, whose tail spreads below the unoccupied  $\uparrow$ -spin  $e'_g$  band. The distribution of the  $e'_g$  states is very similar for all three compounds. Contrary to the metallic state, the orbital ordering is determined not only by local trigonal distortions, but also the form of the superexchange (SE) interactions between  $nn$  Mo sites, and minimizes the energy of these interactions.<sup>34</sup> Generally, it depends on the magnetic state. Two typical examples for the FM and AFM (obtained after the flip of the spin moments at the sites 2 and 3) phases are shown in Figs. 8 and 9, respectively. The building blocks of the AFM phase are the FM chains of the atoms ...-1-4-1-4-.. and ...-2-3-2-3-..., which are coupled antiferromagnetically. As expected for the FM spin ordering,<sup>34</sup> the  $e'_g$  orbitals tends to order "antiferromagnetically" and form two Mo sublattices. Corresponding eigenfunctions of the occupied  $e'_g$  orbitals, obtained after the diagonalization of the density matrix *in the local coordinate frame*, are given by  $|o_{1,4}\rangle \simeq \alpha|xy\rangle + \beta|yz\rangle + \gamma|zx\rangle$  for the sites 1 and 4, and  $|o_{2,3}\rangle \simeq \alpha|xy\rangle + \gamma|yz\rangle + \beta|zx\rangle$  for the sites 2 and 3, with the coefficients  $\alpha \simeq 0.600$ ,  $\beta \simeq 0.193$ , and  $\gamma \simeq -0.769$ . Clearly, this orbital ordering breaks the  $Fm\bar{3}d$  symmetry: if the sites belonging to the same sublattice can still be transformed to each other using the symmetry operations of the  $Fm\bar{3}d$  group, the sites belonging to different sublattices – cannot. This will generally lead to the anisotropy of electronic properties, including the anisotropy of  $nn$  magnetic interactions, which will be discussed in the next section.

The AFM spin ordering coexists with the FM orbital ordering for which  $\alpha \simeq -0.774$ , and  $\beta = \gamma \simeq 0.442$  for all Mo sites, in the local coordinate frame.<sup>36</sup> It breaks the  $Fm\bar{3}d$  symmetry in the spin sector, but not in the orbitals one.

## V. NEAREST-NEIGHBOR EXCHANGE INTERACTIONS

Parameters of exchange interactions between sites  $\tau$  and  $\tau'$  can be calculated as<sup>37</sup>

$$J_{\tau\tau'} = \frac{1}{2\pi} \text{Im} \int_{-\infty}^{\varepsilon_F} d\varepsilon \text{Tr}_L \left\{ \widehat{\mathcal{G}}_{\tau\tau'}^{\uparrow}(\varepsilon) \widehat{\Delta}_{\tau'} \widehat{\mathcal{G}}_{\tau'\tau}^{\downarrow}(\varepsilon) \widehat{\Delta}_{\tau} \right\}, \quad (6)$$

where  $\widehat{\mathcal{G}}_{\tau\tau'}^{\uparrow,\downarrow}(\varepsilon)$  is the block of matrix elements of the Green function with the spin  $\uparrow$  or  $\downarrow$ :

$$\widehat{\mathcal{G}}_{\tau\tau'}^{\uparrow,\downarrow} = \frac{1}{2} \text{Tr}_S \left\{ (\widehat{1} \pm \widehat{\sigma}_z) \widehat{\mathcal{G}}_{\tau\tau'} \right\},$$

and  $\widehat{\Delta}_{\tau}$  is the magnetic part of the HF potential:

$$\widehat{\Delta}_{\tau} = \text{Tr}_S \{ \widehat{\sigma}_z \widehat{\mathcal{U}}_{\tau} \}.$$

$\text{Tr}_{S(L)}$  is the trace running over the spin (orbital) indices.

Results for  $nn$  magnetic interactions for all considered compounds are shown in Fig. 10, as a function of  $U$ . We note the following.

1.  $J_{\tau\tau'}$ , which are ferromagnetic for small  $U$ , exhibit a sharp drop at the point of transition into the insulating state (see Fig. 5 for the behavior of the band gap).
2. There is a significant difference between Nd/Gd and Y based compounds: in the Y case, the exchange parameters are almost rigidly shifted towards negative values, so that the  $nn$  coupling become antiferromagnetic in the insulating phase, while it remains ferromagnetic in the case of Nd and Gd.

Similar conclusions can be obtained from the analysis of total energies shown in Fig. 11.<sup>38</sup>

The behavior can be easily understood by considering partial  $a_{1g}$  and  $e'_g$  contributions to the  $nn$  exchange coupling, calculated after transformation to the local coordinate frame at each site of the system (Fig. 12). Then, the main interactions are  $a_{1g}$ - $a_{1g}$  and  $e'_g$ - $e'_g$ . The  $a_{1g}$ - $e'_g$  interaction is small and can be neglected. The interaction between  $t_{2g}$  and proper  $e_g$  orbitals is of the order of 1.5-1.8 meV and only weakly depends on  $U$  and the type of the material. Therefore, it can be regarded as the weak FM background.

Large FM  $e'_g$ - $e'_g$  interaction in the metallic regime is related with the double exchange (DE) mechanism, which is the measure of the kinetic energy for the itinerant  $\uparrow$ -spin  $e'_g$  electrons (note that for small  $U$  all compounds are either half-metallic or nearly half-metallic –

Fig. 3).<sup>40</sup> Some increase of  $J_{\tau\tau'}$  for small  $U$  is caused by the reduction of AFM SE contributions, which are proportional to  $1/U$ . As long as the system is metallic, the DE interactions are not sensitive to the value of  $U$ , and the FM coupling dominates.

The transition into the insulating state is caused by the localization of the  $e'_g$  electrons on the atomic orbitals. This will reduce the kinetic energy and suppress the DE interactions, that explain the sharp drop of  $J_{\tau\tau'}$  (Fig. 10).

The main difference between Y and Nd/Gd based compounds is related with the  $a_{1g}$ - $a_{1g}$  interactions. Since the  $\uparrow$ -spin  $a_{1g}$  band is fully occupied and the  $\downarrow$ -spin band is empty, the interactions are antiferromagnetic and the underlying microscopic mechanism is the superexchange. Since the SE coupling is proportional to the square of the  $a_{1g}$  bandwidth, this interaction is the largest in the case of Y, that explains the AFM character of the total coupling realized in this compound for large  $U$ .<sup>41</sup>

The anisotropy of the  $nn$  interactions,  $\Delta J = J_{12} - J_{14}$ , caused by the orbital ordering in the FM state is of the order of 1-2 meV (Fig. 10). This is a small value in comparison with the sharp drop of  $J_{\tau\tau'}$  caused by the Coulomb interaction  $U$ . However, it can play an important role in the insulating regime, where  $\Delta J$  becomes comparable with  $J_{\tau\tau'}$ . For example, one interesting question is whether this  $\Delta J$ , of a purely Coulombic origin, is sufficient to explain the appearance of the SG state. In addition,  $\Delta J$  has the same order of magnitude as the single-ion anisotropy energy (Sec. VI) and the Mo-Gd exchange interaction (Ref. 39). Therefore, in the insulating state there is no unique interaction which would control the magnetic behavior of the  $A_2\text{Mo}_2\text{O}_7$  compounds. All interactions are equally important, that represents the main complexity on the way of theoretical description of these materials.

The AFM spin ordering changes the orbital ordering in the direction which further stabilizes the  $nn$  magnetic interactions,<sup>34</sup> and in a number of cases may lead to the charge disproportionation within the FM chains.<sup>42</sup> For example,  $U=2.0$  eV appears to be sufficient to open the band gap ( $\sim 0.3$  eV) in the AFM phase of  $\text{Y}_2\text{Mo}_2\text{O}_7$ . The solution is accompanied by the small charge disproportionation, and the values of the spin magnetic moments at the four Mo sites are  $\mu_1^S = -\mu_3^S = 1.4 \mu_B$  and  $-\mu_2^S = \mu_4^S = 1.5 \mu_B$ . Corresponding values of the inter-atomic exchange interactions are  $J_{12} = -0.8$ ,  $J_{13} = -2.9$  and  $J_{14} = 2.6$  meV, i.e. the interactions are antiferromagnetic in the bonds 1-2 and 1-3, and ferromagnetic in the bond 1-4. Therefore, the obtained solution is locally stable. The difference between  $J_{12}$  and  $J_{13}$  is caused by the charge disproportionation. Further increase of  $U$  stabilizes the AFM cou-

pling in all Mo-Mo bonds, giving rise to the geometrical frustrations. Typical values of the exchange parameters obtained in the HF solution for  $U=3.0$  eV, which does not show any sign of the charge disproportionation, are  $J_{12}=J_{13}=-10.7$  and  $J_{12}=-2.4$  meV.

## VI. NON-COLLINEAR MAGNETIC ORDERING

In this and subsequent sections we will discuss the effects of SOI on the electronic and magnetic structure of the Mo pyrochlores. The matrix element of  $\xi(\mathbf{r})$  calculated in the basis of Mo( $4d$ ) orbitals is of the order of  $\xi_{4d}=120$  meV. It defines the characteristic energy gain after adding the SOI into the model HF Hamiltonian. The equilibrium magnetic ordering depends on the competition between the isotropic exchange interactions, considered in the previous section, and the single-ion anisotropies energy. The isotropic exchange interactions tend to align Mo spins parallel to each other (at least in the case of the FM coupling). However, due to the peculiarities of the pyrochlore structure, there is no unique direction of the spin magnetization which would satisfy the single-ion anisotropy energies simultaneously for all Mo sites. These anisotropies lead to the distortion of the collinear FM ordering.<sup>11</sup>

In the case of FM coupling between  $nn$  spins, there are two magnetic structures, which are typically discussed in the literature and can be obtained by distorting the collinear FM ordering along either  $(0, 0, 1)$  or  $(1, 1, 1)$  direction (see Fig. 13).

1. The "two-in, two-out" structure, where the directions of the magnetic moments at the four Mo sites are given by:  $\mathbf{e}_1 = \frac{1}{\sqrt{1+\eta^4}}(\eta, \eta, 1-\eta^2)$ ,  $\mathbf{e}_2 = \frac{1}{\sqrt{1+\eta^4}}(-\eta, \eta, 1-\eta^2)$ ,  $\mathbf{e}_3 = \frac{1}{\sqrt{1+\eta^4}}(\eta, -\eta, 1-\eta^2)$ , and  $\mathbf{e}_4 = \frac{1}{\sqrt{1+\eta^4}}(-\eta, -\eta, 1-\eta^2)$ , in terms of the distortion  $\eta$  from the perfect FM alignments.
2. The "umbrella" structure:  $\mathbf{e}_1 = \frac{1}{\sqrt{3}}(1, 1, 1)$ ,  $\mathbf{e}_2 = \frac{1}{\sqrt{3(1+2\eta^2)}}(1-2\eta, 1+\eta, 1+\eta)$ ,  $\mathbf{e}_3 = \frac{1}{\sqrt{3(1+2\eta^2)}}(1+\eta, 1-2\eta, 1+\eta)$ , and  $\mathbf{e}_4 = \frac{1}{\sqrt{3(1+2\eta^2)}}(1+\eta, 1+\eta, 1-2\eta)$ .

Since the Mo( $4d$ ) states are strongly polarized by the on-site Coulomb interactions, the main contribution to the single-ion anisotropy energy comes from the  $\uparrow$ -spin electrons. In this case there is an one-by-one correspondence between the single-ion anisotropy energy and the magnitude of the orbital magnetization, so that the direction which maximizes the magnetization automatically minimizes the magnetic anisotropy energy.<sup>43</sup> For the  $t_{2g}$  electrons affected by the trigonal distortion, the spontaneous orbital magnetization is determined by the following factors:<sup>44</sup>

1. The interaction between occupied  $a_{1g}$  and unoccupied  $e'_g$  states favors the in-plane geometry of the orbital magnetization (i.e., perpendicular to the trigonal axes). The latter is proportional to the ratio  $\xi_{4d}/\delta\varepsilon_{a_{1g}}$ , where  $\delta\varepsilon_{a_{1g}}$  is the distance between the position of the  $a_{1g}$  states and the unoccupied part of the spectrum. Clearly, this interaction will vanish when the Coulomb  $U$  is large.
2. On the contrary, the interaction between  $e'_g$  orbitals favors the easy axes geometry. In the pure ionic limit, such solution is the subject for the degenerate perturbation theory. Therefore, the wave functions and the orbital magnetization do not depend on  $\xi_{4d}$ . The SOI in such situation only lifts the orbital degeneracy and defines the symmetry of the  $e'_g$  orbitals which will be further split by  $U$ . The solution is accompanied by the large orbital moment of the order of  $1 \mu_B$ , which is parallel to the trigonal axis.

Thus, when  $U$  is sufficiently large, the second mechanism will dominate and one can naturally expect the easy axes scenario for the single-ion anisotropies. In the combination with the FM coupling between  $nn$  spins, it yields the "umbrella" ground state.<sup>45</sup>

The qualitative analysis is supported by results of direct calculations shown in Fig. 14. In the metallic regime, the isotropic double exchange interaction between Mo spins clearly dominates over the single-ion anisotropy energies and the canting of spin magnetic moments is small (both for the "two-in, two-out" and "umbrella" structure). The orbital moments are not particularly strong ( $<0.1 \mu_B$  per Mo site). They are canted off the global FM direction by about  $10^\circ$ .

In the insulating state, the isotropic exchange interactions are suppressed and become comparable with the single-ion anisotropy energies, which are enhanced. This results in the large canting of the magnetic moments, which can be very different for the spin and orbital counterparts (in the other words, the spin and orbital moments are not collinear with respect to each other).<sup>46,47</sup> The reason for this difference is the following. Directions of the orbital magnetic moments are determined mainly by the single-ion anisotropy terms, whereas the interactions between moments located at different sites are typically much smaller. Therefore, the orbital moments always tend to align first along the crystallographic directions (the trigonal axes, in our case). On the contrary, alignment of the spin magnetic moments is strongly affected by the inter-site interactions, which generally lead to a smaller canting.

For large  $U$  ( $\sim 3$  eV), the single-ion anisotropies start to dominate over the isotropic

exchange interactions. In this limit, the orbital magnetic moments are almost perfectly aligned along the trigonal axes (that corresponds to the 55° and 70° canting for the "two-in, two-out" and "umbrella" structure, respectively). The value of the local orbital magnetic moment is about 0.6  $\mu_B$ , which is smaller than 1  $\mu_B$  expected in the pure atomic limit.

The "umbrella" structure has lower energy (perhaps except the region of very small  $U$ ). The energy difference between the "two-in, two-out" and "umbrella" structures is small in the metallic regime ( $\sim 0.05$  meV per formula unit, which corresponds to the coercive field of 1 Tesla). However, it becomes large in the insulating state, where the interactions between the  $e'_g$  orbitals clearly dominate.

In the case of AFM coupling between  $nn$  spins, the single-ion anisotropies lift, at least partially, the high degeneracy of the magnetic ground state in the frustrated pyrochlore lattice. The equilibrium magnetic structure realized in model HF calculations for  $Y_2Mo_2O_7$  can be obtained by the inversion of the magnetic moments at the sites 2 and 3 of the "two-in, two-out" structure (Fig. 15). For  $U=3.0$  eV, the values of spin and orbital magnetic moments at the Mo sites are 1.44 and 0.51  $\mu_B$ , respectively. They are canted off the cubic (0,0,1) axis by correspondingly 17° and 40°. The AFM interactions are compromised with the tetrahedral geometry of the pyrochlore lattice by forming the AFM coupling between two of the three projections of the  $nn$  spins in each of the Mo-Mo bonds, while the remaining projection is coupled ferromagnetically.

## VII. ANOMALOUS HALL CONDUCTIVITY AND MAGNETO-OPTICAL EFFECT

The conductivity tensor,  $\hat{\sigma}(\omega) = \hat{\sigma}^{\text{reg}}(\omega) + \hat{\sigma}^{\text{D}}(\omega)$ , can be calculated from the eigenvalues,  $\tilde{\varepsilon}_{\mathbf{k}n}$ , and the eigenfunctions,  $|\widetilde{\mathbf{k}n}\rangle$ , of the HF Hamiltonian using the Kubo formula,<sup>49,50</sup> where the inter-band (regular) and intra-band (Drude) contributions are given by (in Ry units)

$$\sigma_{\alpha\beta}^{\text{reg}}(\omega) = \frac{4i}{V} \sum_{\mathbf{k}} \sum_{nn'} \frac{f_{\mathbf{k}n'} - f_{\mathbf{k}n}}{\omega_{n'n}} \left[ \frac{\pi_{nn'}^{\alpha} \pi_{n'n}^{\beta}}{\omega - \omega_{n'n} + i/\tau} + \frac{(\pi_{nn'}^{\alpha} \pi_{n'n}^{\beta})^*}{\omega + \omega_{n'n} + i/\tau} \right] \quad (7)$$

and

$$\sigma_{\alpha\beta}^{\text{D}}(\omega) = \frac{8i}{V} \frac{1}{\omega + i/\tau} \sum_{\mathbf{k}} \sum_n \pi_{nn}^{\alpha} \pi_{nn}^{\beta} \delta(\varepsilon_F - \tilde{\varepsilon}_{\mathbf{k}n}), \quad (8)$$

respectively. In these equations,  $f_{\mathbf{k}n}$  is the zero-temperature Fermi distribution function,  $\pi_{nn'}^{\alpha} = \langle \widetilde{\mathbf{k}n} | (-i\nabla_{\alpha}) | \widetilde{\mathbf{k}n'} \rangle$  is the matrix element of momentum operator,  $\omega_{n'n} = \tilde{\varepsilon}_{\mathbf{k}n'} - \tilde{\varepsilon}_{\mathbf{k}n}$ ,  $V$  is

the unit cell volume, and  $\tau$  is the phenomenological relaxation time ( $1/\tau \simeq 68$  meV) introduces in order to perform summation over the discrete mesh of  $\mathbf{k}$ -points. The diagonal elements of  $\hat{\sigma}^D(\omega)$  can be also expressed through the plasma frequencies,  $\omega_p^\alpha$ , as  $\sigma_{\alpha\alpha}^D = \frac{(\omega_p^\alpha)^2}{4\pi} \frac{i}{\omega + i/\tau}$ .

The conductivity tensor has the form

$$\hat{\sigma} = \begin{pmatrix} \sigma_{xx} & \sigma_{xy} & 0 \\ -\sigma_{xy} & \sigma_{xx} & 0 \\ 0 & 0 & \sigma_{zz} \end{pmatrix}, \quad (9)$$

both for the "two-in, two-out" and "umbrella" structure, if the direction of the  $z$  axis is chosen as  $(0, 0, 1)$  and  $(1, 1, 1)$ , respectively.

The Hall conductivity, defined as  $\sigma_H = \text{Re}\sigma_{xy}(0)$ , is shown in Fig. 16 as a function of  $U$ . As expected,<sup>15</sup> the effect is caused by the inter-band transitions, while all intra-band contributions vanish, even in the metallic state.  $\sigma_H$  takes the maximal value around  $U=1.5$  eV, which compromises between the value of the orbital magnetization and the metallic behavior of the system. On the one hand,  $U$  is large enough to unquench the orbital magnetic moment of the order of  $0.08 \mu_B$  per Mo site. On the other hand it is small enough in order to keep the system in the metallic regime (see Fig. 5). The factor-two increase of  $\sigma_H$  from  $U=0.5$  to 1.5 eV well correlates with similar increase of the orbital magnetic moment (Fig. 14), suggesting that both effects have relativistic origin. The behavior coexists with nearly collinear FM ordering realized in the metallic regime. The transition into the insulating state, which is accompanied by the large canting of the magnetic moments, results in the abrupt drop of  $\sigma_H$ .<sup>48</sup> Therefore, we conclude that the large  $\sigma_H$  observed in the experiment is due to the orbital magnetic moments induced by the SOI in the nearly collinear FM state.<sup>13</sup> The absolute value of  $\sigma_H$ ,  $\sim 25 \Omega^{-1}\text{cm}^{-1}$ , obtained in the calculations is in a good agreement with the experimental data for  $\text{Nd}_2\text{Mo}_2\text{O}_7$ .<sup>1</sup> However, we would like to emphasize again that the SOI alone is not sufficient to obtain such a large values of  $\sigma_H$ , and it is essential to consider the on-site Coulomb interactions beyond LSDA, which play a very important role in the problem and enhance the effect of the SOI.<sup>20</sup>

According to our calculations,  $\sigma_{xy}$ , in the geometry which specify the form of the tensor (9), only weakly depends on the magnetic structure and the direction of the net magnetization. Large anisotropy of  $\sigma_H$  observed in the experiment<sup>1,22</sup> is presumably related with the details of the experimental set-up and reflects the " $\frac{1}{\sqrt{3}}$ -law". For example, if the electric



field is directed along the  $(1, 0, 0)$  axis, and the current is measured along the  $(0, 1, 0)$  axis, the effect is proportional to  $\sigma_{xy}/\sqrt{3}$  in the case of the umbrella structure, that roughly corresponds to the experimental situation. Similar arguments apply for the magneto-optical Kerr rotation which will be discussed below.

If our scenario is correct, and large AHE in the Mo pyrochlores can be explained by the inter-band transitions in the presence of the SOI (i.e., by the conventional means), it is natural to expect similar enhancement for other phenomena related with the SOI. Below we consider the complex Kerr effect, which can be also regarded as a possible check for our theory in the future.

The Kerr rotation ( $\theta_K$ ) and Kerr ellipticity ( $\epsilon_K$ ) can be found from the expression,<sup>51</sup>

$$\frac{1 - \tan \epsilon_K}{1 + \tan \epsilon_K} e^{2i\theta_K} = \frac{1 - n_+}{1 + n_+} \frac{1 + n_-}{1 - n_-}, \quad (10)$$

which is formally exact and valid for arbitrary  $\theta_K$  and  $\epsilon_K$ .  $n_{\pm} = \sqrt{\epsilon_{xx} \pm i\epsilon_{xy}}$  are the complex refractive indices, in terms of matrix elements of the dielectric tensor,  $\epsilon_{\alpha\beta}(\omega) = \delta_{\alpha\beta} + \frac{4\pi i}{\omega} \sigma_{\alpha\beta}(\omega)$ .

Results of these calculations for  $\text{Gd}_2\text{Mo}_2\text{O}_7$  are shown in Fig. 17, together with the  $\omega$ -dependence of the matrix elements of the optical conductivity. We consider the "umbrella" structure obtained for  $U=1.5$  eV, which corresponds to the maximal rotation. Calculations for  $\text{Nd}_2\text{Mo}_2\text{O}_7$  and the "two-in, two-out" structure yield very similar results. We also discuss partial contributions of the  $a_{1g}$  and  $e'_g$  states, and show the spectra obtained after removing the  $a_{1g}$  orbitals from the basis.<sup>52</sup>

Apart from the HF model itself, we do not use any adjustable parameters. For example, the intra-band Drude contribution to the optical conductivity has been obtained in the calculations.

The diagonal part of  $\hat{\sigma}(\omega)$  comes mainly from the inter-band  $e'_g \rightarrow e'_g$  transitions. The contribution of the  $a_{1g}$  states is rather small. The absorptive (Re) part of  $\sigma_{xx}(\omega)$  has a maximum around 1 eV. Both the peak position and its intensity roughly agree with the experimental data,<sup>4</sup> though the latter reveal an additional structure in the low- $\omega$  energy part of the spectrum, which can be due to the quantum fluctuation effects,<sup>53</sup> beyond the mean-field approximation considered in our work.<sup>54</sup>

The contribution of the  $a_{1g}$  states to  $\sigma_{xy}$  is very important, and can bring up to 50% of the spectral weight at certain values of  $\omega$ . However, the low- $\omega$  part of  $\sigma_{xy}$  comes mainly from the

inter-band  $e'_g \rightarrow e'_g$  transitions, which are responsible for almost 90% of the Hall conductivity. The large intensity of  $\sigma_{xy}$  is due to the combination of three factors: (i) large SOI at the Mo sites; (ii) the enhancement of the SOI by the on-site Coulomb interactions, which is especially efficient for the degenerate  $e'_g$  states; (iii) the half-metallic electronic structure of  $\text{Gd}_2\text{Mo}_2\text{O}_7$  and  $\text{Nd}_2\text{Mo}_2\text{O}_7$ : since only  $\uparrow$ -spin states contribute to the low- $\omega$  part of  $\sigma_{xy}$ , the cancellation between different spin channels does not take place.<sup>21</sup>

The Kerr rotation spectrum, calculated using Eq. (10), has two structures. The first one is close to the plasma edge ( $\hbar\omega \simeq 0.3$  eV), and is directly related with the plasma enhancement effect.<sup>51</sup> The exceptionally large value of  $\theta_K$  ( $\sim 8^\circ$ ) is also related with large  $\sigma_{xy}$  in this region, which correlates with the large value of the Hall conductivity. The second structure ( $\theta_K \sim -4^\circ$ ) near 0.7 eV is related with the form of  $\text{Re}\sigma_{xy}(\omega)$ , which has a deep in this region as a joint effect of both  $e'_g \rightarrow e'_g$  and  $a_{1g} \rightarrow e'_g$  inter-band transitions. Smaller  $U$  would yield somewhat smaller estimates for the rotation angles (correspondingly 4 and  $-1.5^\circ$  for  $U=0.5$  eV). Nevertheless, the FM pyrochlores  $A_2\text{Mo}_2\text{O}_7$  seem to be rather promising materials for the magneto-optical applications.

The anomalous Hall and Kerr effects simultaneously vanish in the AFM phase, due to the cancellation of contributions coming from different Mo sublattices in the macroscopic sample.<sup>19</sup>

## VIII. DISCUSSIONS AND SUMMARY

We have presented results of model HF calculations for pyrochlores  $A_2\text{Mo}_2\text{O}_7$  ( $A = \text{Y}, \text{Gd}, \text{and Nd}$ ). The model combines details of LDA electronic structure for the  $\text{Mo}(t_{2g})$  bands located near the Fermi level, the spin-orbit interaction, and the on-site Coulomb interactions amongst the  $\text{Mo}(4d)$  electrons.

The main results can be summarized as follows.

- The magnetic ground state of the  $A_2\text{Mo}_2\text{O}_7$  compounds depends on the Mo-Mo distance, which controls the strength of AFM SE interactions between the  $a_{1g}$  orbitals. The latter competes with the FM interactions between the  $e'_g$  orbitals, and dominates when the Mo-Mo distance is small. In the frustrated pyrochlore lattice, this corresponds to the transition into the SG state, though we cannot specify precisely which mechanism freeze the random configuration of the Mo spins. It could be the disorder of the Mo-Mo bondlengths proposed

in Refs. 9 and 10. Another possibility is the anisotropy of nearest-neighbor magnetic interactions caused by the orbital ordering.<sup>55</sup> It is also important to note that the Coulomb repulsion  $U$  should be sufficiently strong in order to open the band gap and suppress the FM double exchange interactions between the  $e'_g$  orbitals.

- The metal-insulator transition in these systems does not necessarily coincide with the FM-SG transitions. All metallic compounds are expected to be nearly collinear ferromagnets, due to the double exchange mechanism. However, the inter-atomic exchange coupling in the insulating state can be both ferromagnetic and antiferromagnetic, depending on the Mo-Mo bondlength. The finding is qualitatively consistent with the experimental data.<sup>5</sup> The magnetic structure in the insulating state is expected to be strongly non-collinear, due to the competition between the isotropic exchange interactions and the single-ion anisotropies.

- The large Hall conductivity can be explained by the combination of three factors in the nearly collinear FM state: large SOI at the Mo sites, which unquenches the orbital magnetization; strong enhancement of this effect by the on-site Coulomb interaction; and the half-metallic electronic structure of the FM pyrochlores. We also expect large magneto-optical effect in the same compounds.

A possible way to enhance these properties is to use heavy  $5d$  elements, which have large spin-orbit coupling. Unfortunately, all known  $5d$  pyrochlores are non-magnetic, though some of them are presumably close to the point of magnetic instability.<sup>32</sup> Nevertheless, one can try to exploit an old idea known from the physics of intermetallic alloys,<sup>56</sup> and replace part of the Mo sites in  $A_2\text{MoO}_7$  by the  $5d$  elements. Then, the main question is whether the remaining Mo sites will be magnetic in the new environment or not. If they will, they will also magnetize the  $5d$  states at the neighboring sites, and in this way enhance the non-reciprocal characteristics of the considered pyrochlore compounds. As a purely model example, we have considered the ordered  $\text{Gd}_2\text{MoWO}_7$  alloy (using the lattice parameters of  $\text{Gd}_2\text{Mo}_2\text{O}_7$ ). According to the LSDA calculations, the system is expected to be ferromagnetic. The values of (spin only) magnetic moments at the Mo and W sites are  $2.1$  and  $1.5 \mu_B$ , respectively. The situation is highly unusual, because the examples when  $4d$  and  $5d$  elements form a magnetic solution are rather rare. Although  $\text{Gd}_2\text{MoWO}_7$  itself may be rather unrealistic example from the technological point of view, the idea to use Mo atoms in order to magnetize the heavy  $5d$  elements in the pyrochlore lattice seems to be promising.

In conclusion, the simple HF calculations allow to rationalize many unusual properties of

the pyrochlore compounds  $A_2\text{Mo}_2\text{O}_7$ . It is also important that all these properties can be explained by the universal value of  $U \sim 1.5\text{-}2.5$  eV, which is of the same order of magnitude as the characteristic bandwidth for the  $\text{Mo}(t_{2g})$  electrons. This will certainly place the considered compounds to the direct proximity of the metal-insulator transition, meaning that the quantum fluctuations beyond the mean-field HF approach will play an important role too. This is certainly a very important direction for the extension of the present analysis.

Finally, we would like to make several comments on the comparison between our calculations and the experimental magnetization<sup>1,22,57</sup> and neutron diffraction<sup>1,58</sup> data.

(1) The experimental value of the Mo moment ( $\sim 1.1\text{-}1.3 \mu_B$ ) seems to be smaller than  $\sim 1.4 \mu_B$  obtained in our mean-field calculations for the nearly collinear FM state, even after taking into account the orbital part ( $\sim 0.1 \mu_B$ ), which according to the third Hund's rule is antiparallel to the spin one and partly compensate the latter. The small difference is presumably related with the quantum fluctuations at the proximity of the metal-insulator transition.<sup>59</sup>

(2) The experimental data for  $\text{Nd}_2\text{Mo}_2\text{O}_7$  and  $\text{Sm}_2\text{Mo}_2\text{O}_7$  typically indicate at the existence of two antiferromagnetically coupled sublattices. These sublattices are usually regarded as Mo and A ones. However, according to the electronic structure point of view, the *spin* coupling between these two sublattices should be ferromagnetic,<sup>39</sup> being actually consistent with the experimental data for  $\text{Gd}_2\text{Mo}_2\text{O}_7$ .<sup>57</sup> The controversies can be reconciled with each other if the local magnetic moment at the Nd/Sm sites has a large orbital counterpart, which is larger than the spin one. The AFM orientation of the spin and orbital moments at the Nd/Sm sites is again the subject of the third Hund's rule. Then, the magnetization and neutron diffraction experiments presumably probe the AFM coupling between *spin* magnetic moments at the Mo sites and the *orbital* magnetic moments at the Nd/Sm sites.  $\text{Gd}^{3+}$  has no orbital moment, and therefore the experimental data for this compound indicate at the conventional FM coupling between two spin sublattices. Then, the sharp decrease of the magnetization observed in  $\text{Nd}_2\text{Mo}_2\text{O}_7$  at low  $T$ ,<sup>1</sup> which is frequently tempted to connect with the anomaly of the Hall conductivity is due to the orbital magnetic structure, not the spin one. The change of the *orbital* magnetic structure seems to be the right subject to concentrate at when trying to explain, for example, the temperature dependence of the AHE. In this respect, another interesting problem seems to be the behavior of *spin and orbital* magnetic moments at the Mo sites, because already in the ground state these two

sublattices from mutually non-collinear magnetic structures. Therefore, it is reasonable to expect very unconventional spin and orbital dynamic at the elevated temperatures.

### Acknowledgments

I would like to thank Lars Nordström for collaboration on early stages of this project and kind hospitality during my stay at Uppsala University. I also benefited from discussions with N. Nagaosa, Y. Tokura, K. Terakura, and A. B. Granovski.

---

\* Electronic address: igor.solovyev@aist.go.jp

- <sup>1</sup> Y. Taguchi, Y. Oohara, H. Yoshizawa, N. Nagaosa, and Y. Tokura, *Science* **291**, 2573 (2001).
- <sup>2</sup> T. Katsufuji, H. Y. Hwang, and S-W. Cheong, *Phys. Rev. Lett.* **84**, 1998 (2000).
- <sup>3</sup> Y. Moritomo, Sh. Xu, A. Machida, T. Katsufuji, E. Nishibori, M. Takata, M. Sakata, and S-W. Cheong, *Phys. Rev. B* **63**, 144425 (2001).
- <sup>4</sup> Y. Taguchi, K. Ohgushi, and Y. Tokura, *Phys. Rev. B* **65**, 115102 (2002).
- <sup>5</sup> S. Iikubo, S. Yoshii, T. Kageyama, K. Oda, Y. Kondo, K. Murata, and M. Sato, *J. Phys. Soc. Jpn.* **70**, 212 (2001).
- <sup>6</sup> J. N. Reimers, J. E. Greedan, and M. Sato, *J. Solid State Chem.* **72**, 390 (1988).
- <sup>7</sup> J. S. Gardner, B. D. Gaulin, S.-H. Lee, C. Broholm, N. P. Raju, and J. E. Greedan, *Phys. Rev. Lett.* **83**, 211 (1999).
- <sup>8</sup> J. N. Reimers, *Phys. Rev. B* **45**, 7287 (1992).
- <sup>9</sup> C. H. Booth, J. S. Gardner, G. H. Kwei, R. H. Heffner, F. Bridges, and M. A. Subramanian, *Phys. Rev. B* **62**, R755 (2000).
- <sup>10</sup> A. Keren and J. S. Gardner, *Phys. Rev. Lett.* **87**, 177201 (2001).
- <sup>11</sup> T. Moriya, *Phys. Rev.* **117**, 635 (1960).
- <sup>12</sup> J. Ye, Y. B. Kim, A. J. Millis, B. I. Shraiman, P. Majumdar, and Z. Tešanovich, *Phys. Rev. Lett.* **83**, 3737 (1999). Y. Lyanda-Geller, S. H. Chun, M. B. Salamon, P. M. Goldbart, P. D. Han, Y. Tomioka, A. Asamitsu, and Y. Tokura, *Phys. Rev. B* **63**, 184426 (2001).
- <sup>13</sup> R. Karplus and J. M. Luttinger, *Phys. Rev.* **95**, 1154 (1954).
- <sup>14</sup> J. Smith, *Physica* **21**, 877 (1955); J. Smith, *ibid.* **24**, 39 (1958); J. M. Luttinger, *Phys. Rev.* **112**,

739 (1958); J. Kondo, Prog. Theor. Phys. **27**, 772 (1962); F. E. Maranzana, Phys. Rev. **160**, 421 (1967); L. Berger, Phys. Rev. B **2**, 4559 (1970); L. Berger, *ibid.* **5**, 1862 (1972); S. K. Lyo and T. Holstein, Phys. Rev. Lett. **29**, 423 (1972); J. Smith, Phys. Rev. B **17**, 1450 (1978).

<sup>15</sup> We would not like to go here very deeply into all details of these controversies. Briefly, Karplus and Luttinger in their pioneering work<sup>13</sup> considered the contributions proportional to  $\partial f/\partial \varepsilon$ , where  $f$  is the Fermi distribution function. These contributions have the form of intra-band transitions in the conductivity tensor depicted by Eq. (8). All of them vanish in the periodic crystal, as it was correctly pointed out by Smith.<sup>14</sup> However, if the product of two momentum operators,  $\pi_{nn'}^\alpha \pi_{n'n}^\beta$ , has an imaginary part, one can expect another contribution to  $\sigma_H$  coming from Eq. (7). This contribution is caused by the inter-band transitions, and in this sense the considered mechanism has the same origin as the magneto-optical effect. This term was intensively studied recently by Nagaosa *et al.* in the context of the spin-chirality problem.<sup>18</sup> See also comments in Ref. 17.

<sup>16</sup> A. B. Granovskiy and Ye. I. Kondorskiy, Fiz. Metal. Metalloved. **39**, 718 (1975) [English transl.: The Physics of Metals and Metallography **39**, No.4, p.36 (1975)]; Ye. I. Kondorskiy, A. V. Vedyayev, and A. B. Granovskiy, *ibid.* **40**, 455 (1975) [English transl.: The Physics of Metals and Metallography **40**, No.3, p.1 (1975)]; N. Ryzhanova, A. Vedyayev, A. Crépieux, and C. Lacroix, Phys. Rev. B **57**, 2943 (1998).

<sup>17</sup> Using expression (7) for the conductivity tensor, it is easy to show that  $\sigma_{\alpha\beta}^*(\omega) = \sigma_{\alpha\beta}(-\omega)$ . Therefore,  $\text{Im}\sigma_{\alpha\beta}(0) = 0$ , whereas  $\sigma_H \equiv \text{Re}\sigma_{\alpha\beta}(0)$  can be finite (the author thank N. Nagaosa for pointing out this property). On the other hand, the Onsager constraint  $\sigma_{\alpha\beta}(\omega, \mu) = \sigma_{\beta\alpha}(\omega, -\mu)$  ( $\mu$  being the net magnetization) requires  $\sigma_H$  to be an even function of  $\mu$ .<sup>60</sup> Strictly speaking, the effect is masked by the diagonal elements of the conductivity tensor, and since  $\text{Re}\sigma_{xx}(0) \rightarrow \infty$ , the resistivity  $\rho_{xy} = -\text{Re}\sigma_{xy}(0)/\text{Re}\sigma_{xx}^2(0)$ , which is the measured quantity, will vanish anyway in the perfectly periodic metallic state. In this sense, additional scattering mechanisms<sup>14,16</sup> are indispensable in order to have finite  $\text{Re}\sigma_{xx}(0)$  and  $\rho_{xy}$ . However, it does not mean that  $\text{Re}\sigma_{xy}(0)$  itself will vanish in the periodic state. In our work we will consider such, perhaps somewhat idealistic, situation.

<sup>18</sup> K. Ohgushi, S. Murakami, and N. Nagaosa, Phys. Rev. B **62**, R6065 (2000); R. Shindou and N. Nagaosa, Phys. Rev. Lett. **87**, 116801 (2001); M. Onoda and N. Nagaosa, J. Phys. Soc. Jpn. **71**, 19 (2001).

- <sup>19</sup> I. E. Dzyaloshinskii, Phys. Lett. A **155**, 62 (1991); I. Dzyaloshinskii and E. V. Papamichail, Phys. Rev. Lett. **75**, 3004 (1995).
- <sup>20</sup> I. V. Solovyev, A. I. Liechtenstein, and K. Terakura, Phys. Rev. Lett. **80**, 5758 (1998).
- <sup>21</sup> V. Yu. Irkhin and M. I. Katsnel'son, Usp. Fiz. Nauk **164**, 705 (1994) [English transl.: Physics–Uspekhi **37**, 659 (1994)].
- <sup>22</sup> S. Yoshii, S. Iikubo, T. Kageyama, K. Oda, Y. Kondo, K. Murata, and M. Sato, J. Phys. Soc. Jpn. **69**, 3777 (2002).
- <sup>23</sup> Y. Taguchi and Y. Tokura, Phys. Rev. B **60**, 10280 (1999).
- <sup>24</sup> D. J. Singh, J. Appl. Phys. **79**, 4818 (1996).
- <sup>25</sup> In the local coordinate frame, the  $a_{1g}$  and two  $e'_g$  orbitals have the following form:  $|a_{1g}\rangle = \frac{1}{\sqrt{3}}(|xy\rangle + |yz\rangle + |zx\rangle)$ ,  $|e'_{g1}\rangle = \frac{1}{\sqrt{2}}(|yz\rangle - |zx\rangle)$ , and  $|e'_{g2}\rangle = \frac{1}{\sqrt{6}}(-2|xy\rangle + |yz\rangle + |zx\rangle)$ .
- <sup>26</sup> In this sence, the physics is similar to the spinel compounds: V. I. Anisimov, M. A. Korotin, M. Zöfl, T. Pruschke, K. Le Hur, and T. M. Rice, Phys. Rev. Lett. **80**, 5758 (1998). Note, however, that the oxygen coordination is very different in the spinel and pyrochlore structure.
- <sup>27</sup> I. V. Solovyev, P. H. Dederichs, and V. I. Anisimov, Phys. Rev. B **50**, 16861 (1994).
- <sup>28</sup> I. Solovyev, N. Hamada, and K. Terakura, Phys. Rev. B **53**, 7158 (1996).
- <sup>29</sup> O. K. Andersen, Phys. Rev. B **12**, 3060 (1975); O. Gunnarsson, O. Jepsen, and O. K. Andersen, *ibid.* **27**, 7144 (1983).
- <sup>30</sup> N. Hamada, H. Sawada, and K. Terakura (unpublished).
- <sup>31</sup> L. Nordström, to be published.
- <sup>32</sup> D. J. Singh, P. Blaha, K. Schwarz, and J. O. Sofo, Phys. Rev. B **65**, 155109 (2002).
- <sup>33</sup> I. V. Solovyev and K. Terakura, Phys. Rev. B **58**, 15496 (1998).
- <sup>34</sup> K. I. Kugel and D. I. Khomskii, Usp. Fiz. Nauk **136**, 621 (1982) [Sov. Phys. Usp. **25**, 231 (1982)].
- <sup>35</sup> By considering the  $nn$  hoppings between Mo( $a_{1g}$ ) orbitals in the pyrochlore lattice,  $t_{a_{1g}}$ , it is easy to show that the electronic structure for the  $a_{1g}$  states will consist of three bands (in units of  $t_{a_{1g}}$ ):  $\varepsilon_{\mathbf{k}\pm} = -2 \pm \sqrt{1 + s_{\mathbf{k}}}$ , the so-called bonding and antibonding bands, and the doubly-degenerate non-bonding band  $\varepsilon_{\mathbf{k}0} = 2$ , where  $s_{\mathbf{k}} = \cos \frac{k_x a}{2} \cos \frac{k_y a}{2} + \cos \frac{k_y a}{2} \cos \frac{k_z a}{2} + \cos \frac{k_z a}{2} \cos \frac{k_x a}{2}$ .
- <sup>36</sup> In fact, there is a non-spherical (proportional to the Coulomb parameter  $B$ ) interaction between occupied  $e'_g$  and  $a_{1g}$  orbitals, which will deforms the density of the  $a_{1g}$  electrons. This interaction has an appreciable effect in the AFM state. For example, for  $\text{Y}_2\text{Mo}_2\text{O}_7$  and  $U=3.0$  eV, the

occupied  $a_{1g}$  orbital at the site 1 has the form  $|a_{1g}\rangle = \alpha|xy\rangle + \beta|yz\rangle + \beta|zx\rangle$ , where  $\alpha \simeq 0.629 \neq \beta \simeq 0.549$ . This will also lead to a small (less than 1 meV) anisotropy of the  $a_{1g}$ - $a_{1g}$  superexchange interactions.

<sup>37</sup> A. I. Liechtenstein, M. I. Katsnelson, V. P. Antropov, and V. A. Gubanov, *J. Magn. Magn. Mater.* **67**, 65 (1987).

<sup>38</sup> Note that  $J_{\tau\tau'}$  defined by Eq. (6), which is basically the second derivative of the total energy,<sup>37</sup> characterizes the *local stability* of the magnetic state, and provides a *complementary* information to the standard total energy calculations. Generally, the parameters  $J_{\tau\tau'}$  depend on the magnetic state in which they are calculated and there is no simple relation between  $J_{\tau\tau'}$  and the total energy. On the other hand, the total energy difference calculated for a limited number of magnetic states does not necessary guarantee that these states are locally stable to be the local minima of the total energy.

<sup>39</sup> The Gd( $4f$ ) core spin polarizes the valence, mainly Gd( $5d$ ), electrons, which can interact with the Mo( $4d$ ) electrons. According to our estimates based on Eq. 6, the interaction  $J_{5d-4d}$  is ferromagnetic and is of the order of 2 meV (in LSDA, and treating the Gd( $4f$ ) states as the core states), in a good agreement with the experimental data.<sup>57</sup> Similar conclusion can be obtained from the analysis of the total energy difference, assuming the FM and AFM coupling between Mo and Gd spins. Results of these calculations have very transparent explanation, because Gd<sub>2</sub>Mo<sub>2</sub>O<sub>7</sub> has half-metallic electronic structure and the FM coupling between Mo and Gd spins results in the additional energy gain for the  $\uparrow$ -spin Mo( $t_{2g}$ ) electrons (see Fig. 3). For comparison, the direct Gd( $5d$ )-Gd( $5d$ ) interaction is much smaller ( $\sim 0.03$  meV, which is formally beyond the accuracy verge of the present calculations).

<sup>40</sup> I. V. Solovyev and K. Terakura, to be published in *Electronic Structure and Magnetism of Complex Materials*, ed. by D. J. Singh (Springer-Verlag, Berlin, 2002).

<sup>41</sup> Presumably, other factors can also play some role in explaining the large difference of  $a_{1g}$ - $a_{1g}$  interactions obtained for Y<sub>2</sub>Mo<sub>2</sub>O<sub>7</sub> and Nd<sub>2</sub>Mo<sub>2</sub>O<sub>7</sub>. The standard SE interaction is proportional to the (minus) second moment of the density of states, that actually explains the AFM sign of the coupling.<sup>40</sup> The  $\uparrow$ -spin  $a_{1g}$  bandwidths in Y<sub>2</sub>Mo<sub>2</sub>O<sub>7</sub> and Nd<sub>2</sub>Mo<sub>2</sub>O<sub>7</sub> differ by factor two (Fig. 7), that should lead to the factor four difference for corresponding SE interactions. However, the  $a_{1g}$  states are not fully isolated and interact with some other states, so that the expression for the SE interaction should be modified as  $J^S \propto \text{Im} \int_{-\infty}^{\epsilon_F} d\epsilon (\epsilon - c_{\uparrow})(\epsilon - c_{\downarrow}) \text{Tr}_L \mathcal{G}_{\tau\tau}^{\uparrow}(\epsilon)$ , where  $c_{\uparrow, \downarrow}$  is



the shift of the  $a_{1g}$  states due to the hybridization with other states. This shift can be different for the  $\uparrow$ - and  $\downarrow$ -spin electrons and also depend on the material, that presumably explains an additional difference between  $\text{Y}_2\text{Mo}_2\text{O}_7$  and  $\text{Nd}_2\text{Mo}_2\text{O}_7$ .

- <sup>42</sup> Note that at least in the mean-field approximation for the one-orbital model, the effects of the inter-site Coulomb interactions, which are responsible for the charge disproportionation, can be included as a renormalization of the local (on-site) interaction, in the spirit of model HF calculations performed in this work: I. V. Solovyev, Phys. Rev. B **60**, 8550 (1999).
- <sup>43</sup> P. Bruno, Phys. Rev. B **39**, 865 (1989).
- <sup>44</sup> I. V. Solovyev, A. I. Liechtenstein, and K. Terakura, J. Magn. Magn. Matter. **185**, 118 (1998).
- <sup>45</sup> The conclusion can be easily verified by considering the spin Hamiltonian  $\mathcal{H}_S = -J \sum_{\langle \tau \tau' \rangle} (\mathbf{e}_\tau, \mathbf{e}_{\tau'}) + \sum_\tau (\mathbf{e}_\tau, \hat{\mathbb{D}}_\tau \mathbf{e}_\tau)$ , consisting of the  $nn$  exchange and anisotropy parts.  $\mathbb{D}_1 = d \|\frac{2}{3} \delta_{\alpha\beta} - 1\|$  is the single-ion anisotropy tensor at the site 1.  $\hat{\mathbb{D}}_2$ ,  $\hat{\mathbb{D}}_3$ , and  $\hat{\mathbb{D}}_4$  are obtained by the  $180^\circ$  rotations of  $\hat{\mathbb{D}}_1$  around  $x$ ,  $y$ , and  $z$ , respectively. Then if  $J > 0$  (the FM coupling) and  $d > 0$  (the easy axes scenario), the "umbrella" structure has lower energy in comparison with the "two-in, two-out" structure due to the additional energy gain coming from the  $nn$  exchange interactions.
- <sup>46</sup> L. M. Sandratskii and J. Kübler, Phys. Rev. Lett. **76**, 4963 (1996).
- <sup>47</sup> I. V. Solovyev, Phys. Rev. B **55**, 8060 (1997).
- <sup>48</sup> Note that  $\sigma_H \propto \delta_G^{-2}$ , where  $\delta_G$  is the band gap. In addition, the non-collinear alignment reduces the net magnetization and the conventional contribution to the AHE caused by the SOI.<sup>13</sup>
- <sup>49</sup> Yu. A. Uspenski, E. G. Maksimov, S. N. Rashkeev, and I. I. Mazin, Z. Phys. B **53**, 263 (1983).
- <sup>50</sup> C. S. Wang and J. Callaway, Phys. Rev. B **9**, 4897 (1974); Yu. A. Uspenski and S. V. Khalilov, Zh. Eksp. Teor. Fiz. **95**, 1022 (1989) [English transl.: Sov. Phys. JETP **68**, 588 (1989)]; P. M. Oppeneer, T. Maurer, J. Sticht, and J. Kübler, Phys. Rev. B **45**, 10924 (1992).
- <sup>51</sup> R. Pittini, J. Schoenes, O. Vogt, and P. Wachter, Phys. Rev. Lett. **77**, 944 (1996). Yu. A. Uspenskii and B. N. Harmon, Appl. Phys. Lett. **74**, 1618 (1999).
- <sup>52</sup> In practical calculations, we replace the wave functions  $|\widetilde{n\mathbf{k}}\rangle$  by  $(1 - \hat{P}_{a_{1g}})|\widetilde{n\mathbf{k}}\rangle$ , where  $\hat{P}_{a_{1g}}$  is the projection operator onto the  $a_{1g}$  states.
- <sup>53</sup> Y. Tokura and N. Nagaosa, Science **288**, 462 (2000).
- <sup>54</sup> Another possibility could be the sample purity. However, according to the experimental estimates the sample quality seems to be good (for example in  $\text{Y}_2\text{Mo}_2\text{O}_7$  the concentration of

anti-site defects and deviation from the nominal oxygen stoichiometry was estimated as 4% and 1%, respectively).<sup>10</sup>

- <sup>55</sup> Strictly speaking, two mechanisms are closely related because the orbital ordering will produce the lattice distortion and vice versa.
- <sup>56</sup> I. V. Solovyev, P. H. Dederichs, and I. Mertig, *Phys. Rev. B* **52**, 13419 (1995).
- <sup>57</sup> N. Ali, M. P. Hill, S. Labroo, and J. E. Greedan, *J. Solid State Chem.* **83**, 178 (1989).
- <sup>58</sup> Y. Yasui, Y. Kondo, M. Kanada, M. Ito, H. Harashina, M. Sato, and K. Kakurai, *J. Phys. Soc. Jpn.* **70**, 284 (2001).
- <sup>59</sup> Another indication that the FM pyrochlores may not be quite conventional metals is the relatively high resistivity ( $\sim 10^{-3} \Omega\text{cm}$ ).<sup>4</sup>
- <sup>60</sup> D. L. Landau and E. M. Lifshitz, *Electrodynamics of Condensed Media* (Pergamon, New York, 1960).

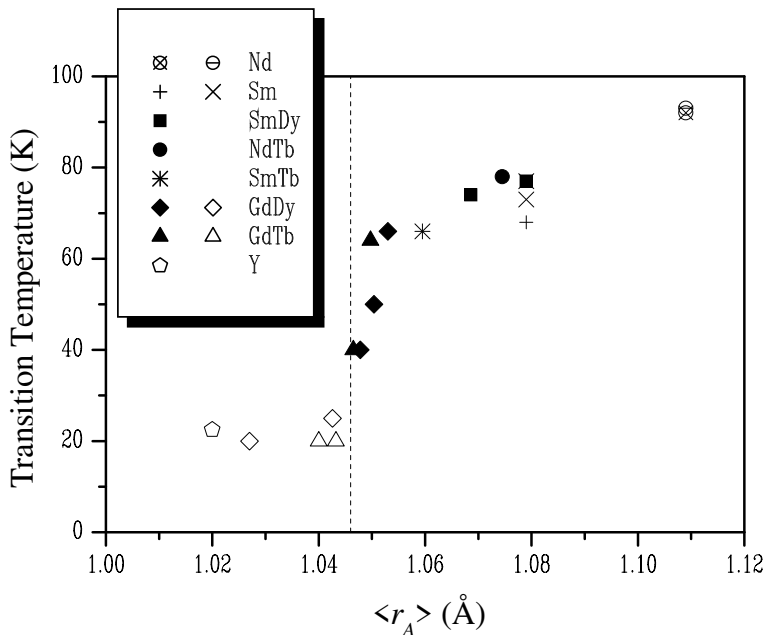
TABLE I: Structural parameters of  $A_2\text{Mo}_2\text{O}_7$  ( $A = \text{Y}, \text{Nd}, \text{and Gd}$ ): the cubic lattice parameter  $a$  (in Å), positions of O 48f sites  $[u, \frac{1}{8}, \frac{1}{8}]$  (units of  $a$ ), the distances Mo-Mo and Mo-O (in Å), and the angles Mo-O-Mo and O-Mo-O (in degrees).

compound	$a$	$u$	$d_{\text{Mo-Mo}}$	$d_{\text{Mo-O}}$	$\angle\text{Mo-O-Mo}$	$\angle\text{O-Mo-O}$
$\text{Y}_2\text{Mo}_2\text{O}_7^a$	10.21	0.33821	3.6098	2.0171	127.0	99.5
$\text{Gd}_2\text{Mo}_2\text{O}_7^b$	10.3356(1)	0.33158	3.6542	2.0123	130.4	97.2
$\text{Nd}_2\text{Mo}_2\text{O}_7^c$	10.4836(2)	0.32977	3.7065	2.0332	131.4	96.6

<sup>a</sup>Ref. 6,  $a$  is from Ref. 7 (corresponding to 4K).

<sup>b</sup>Ref. 3.

<sup>c</sup>Ref. 3.



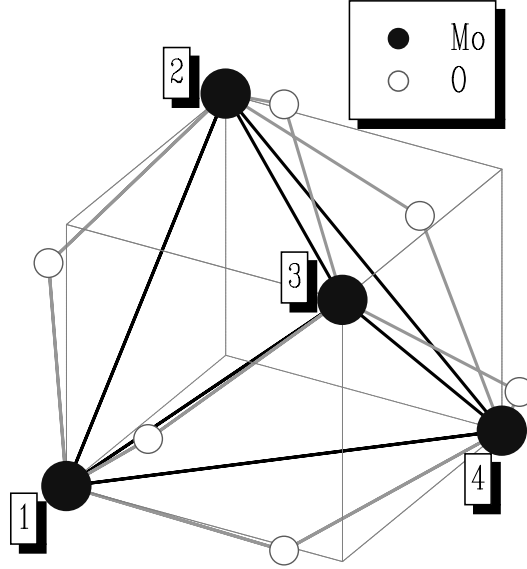


FIG. 2: Relative position of the Mo and O 48*f* sites in pyrochlore lattice.

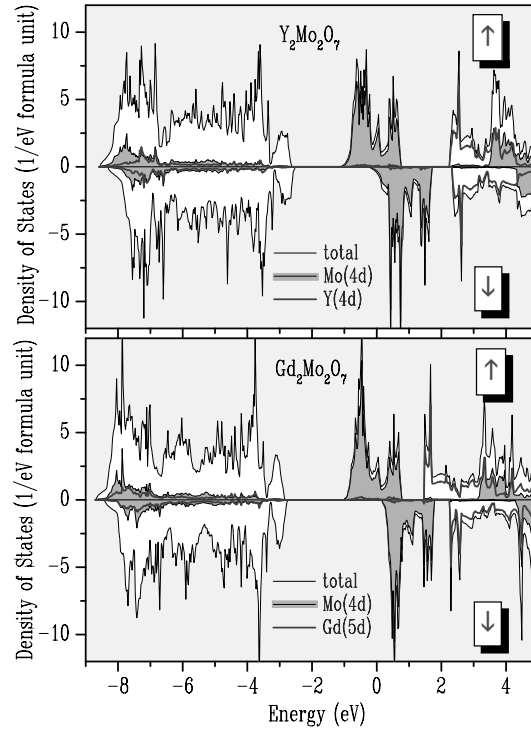


FIG. 3: Total and partial densities of states of  $\text{Y}_2\text{Mo}_2\text{O}_7$  and  $\text{Gd}_2\text{Mo}_2\text{O}_7$  in the local-spin-density approximation. The  $\text{Mo}(t_{2g})$  states are located near the Fermi level (chosen as zero of energy). The  $\text{Mo}(e_g)$  states emerge around 4 eV.

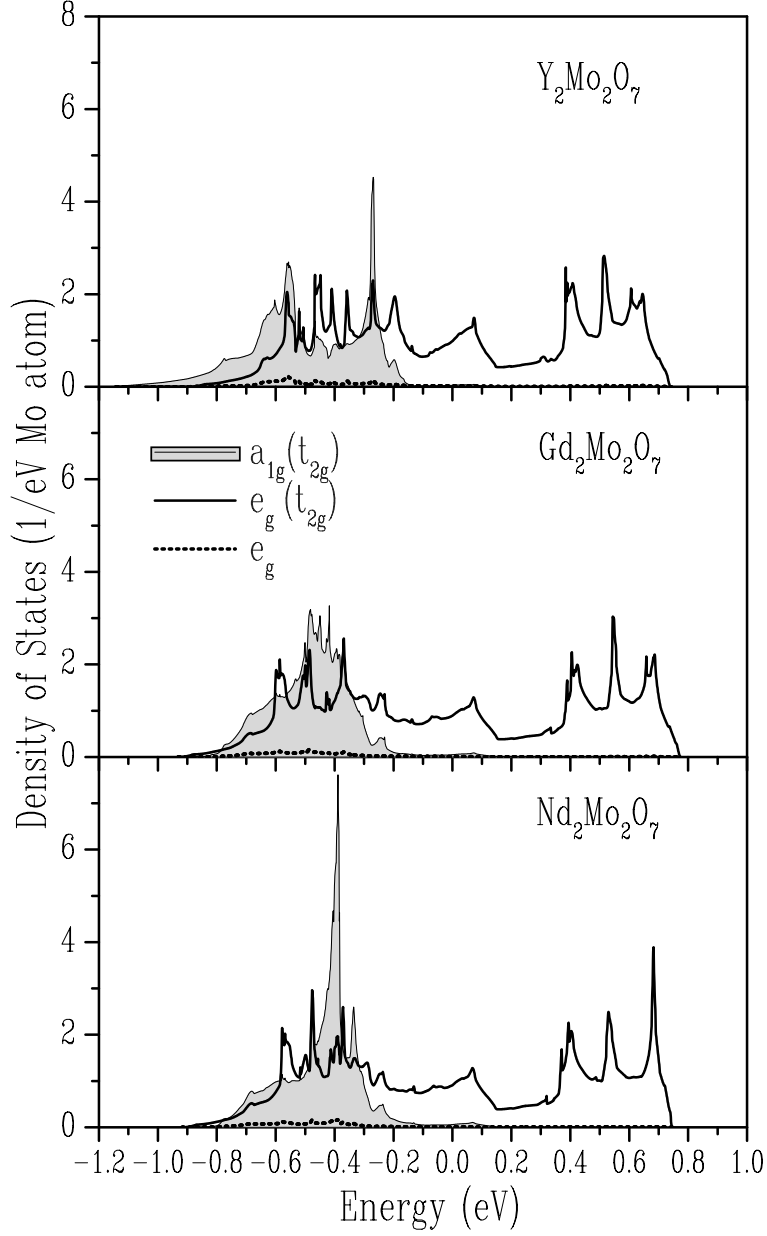


FIG. 4: Mo( $t_{2g}$ ) states in the local coordinate frame, split into the one-dimensional  $a_{1g}$  and two-dimensional  $e'_g$  (denoted as  $e_g(t_{2g})$ ) representations by the local trigonal distortion. The Fermi level is at zero. The contribution of proper  $e_g$  states to this region is small.

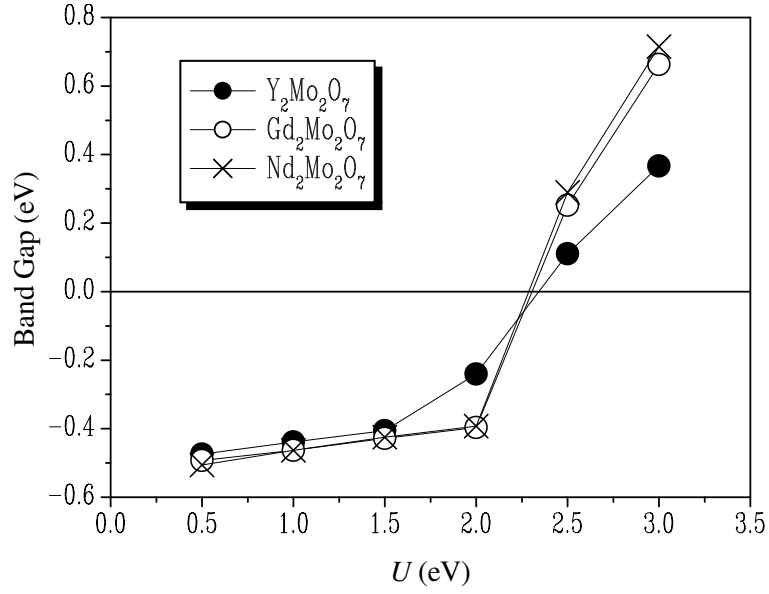


FIG. 5: The band gap as a function of Coulomb  $U$ . Here, the band gap is defined as the distance between the bottom of 9th and the top 8th band, so that for  $U \leq 2.0$  eV there is an overlap between these two bands, corresponding to the negative value of the band gap, while  $U \geq 2.5$  eV opens the real gap.

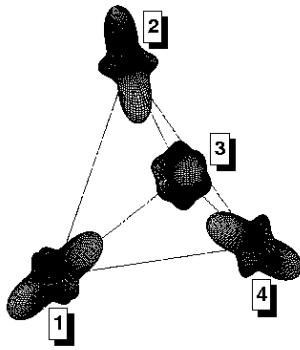


FIG. 6: Orbital ordering in the ferromagnetic phase of  $\text{Y}_2\text{Mo}_2\text{O}_7$  obtained for  $U=0.5$  eV.

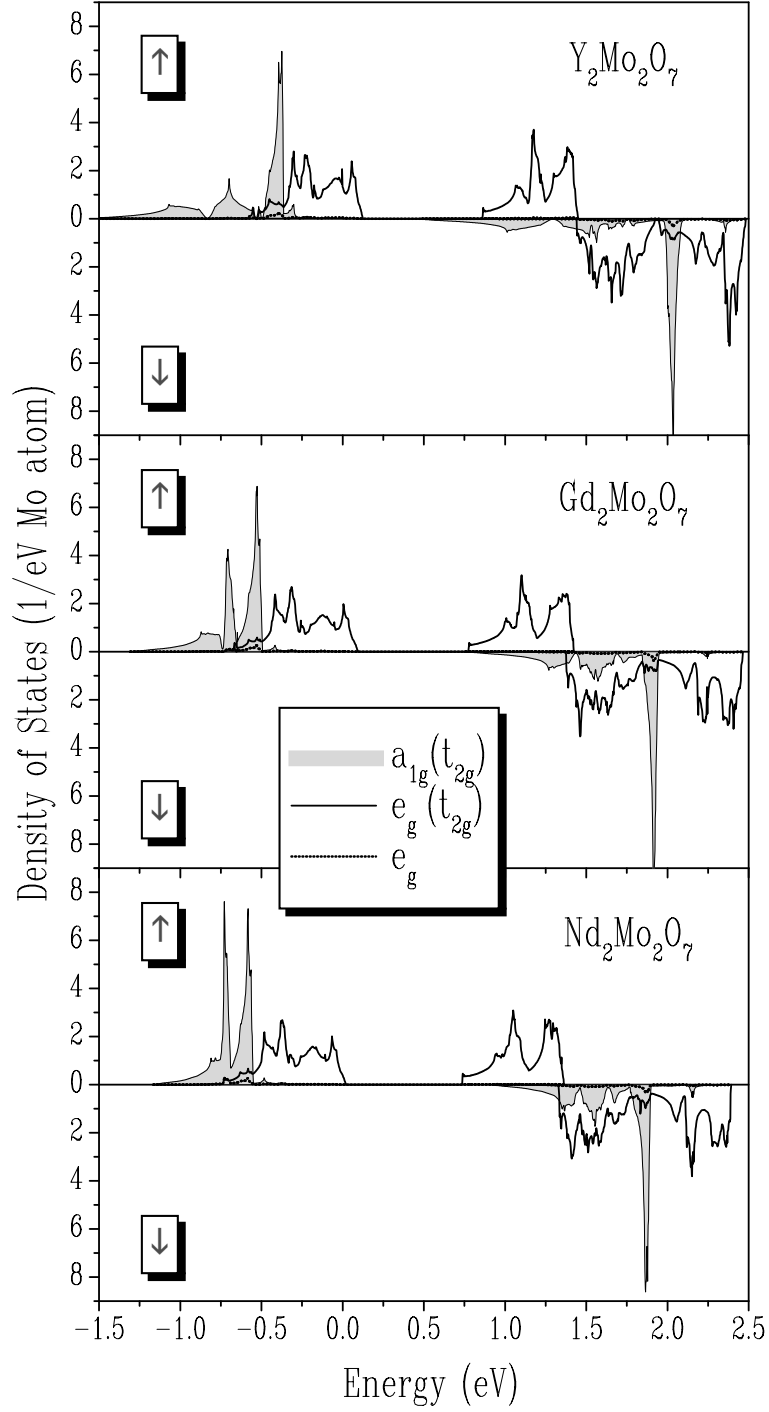


FIG. 7: Distribution of the Mo(4d) states obtained in model Hartree-Fock approach for  $U = 3.0$  eV.



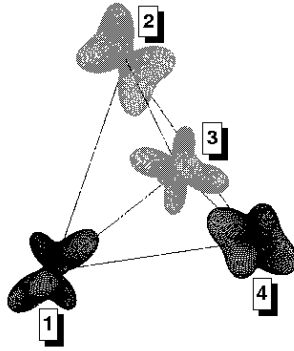


FIG. 8: Orbital ordering in the ferromagnetic phase of  $Y_2Mo_2O_7$  obtained for  $U=3.0$  eV. Two orbital sublattices are shown by black and grey colors.

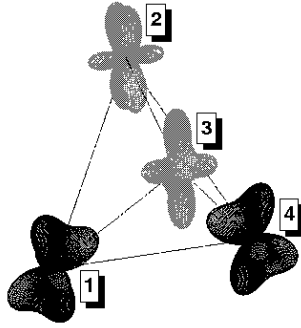


FIG. 9: Orbital ordering in the antiferromagnetic phase of  $\text{Y}_2\text{Mo}_2\text{O}_7$  obtained for  $U=3.0$  eV. Two spin sublattices are shown by black and grey colors.

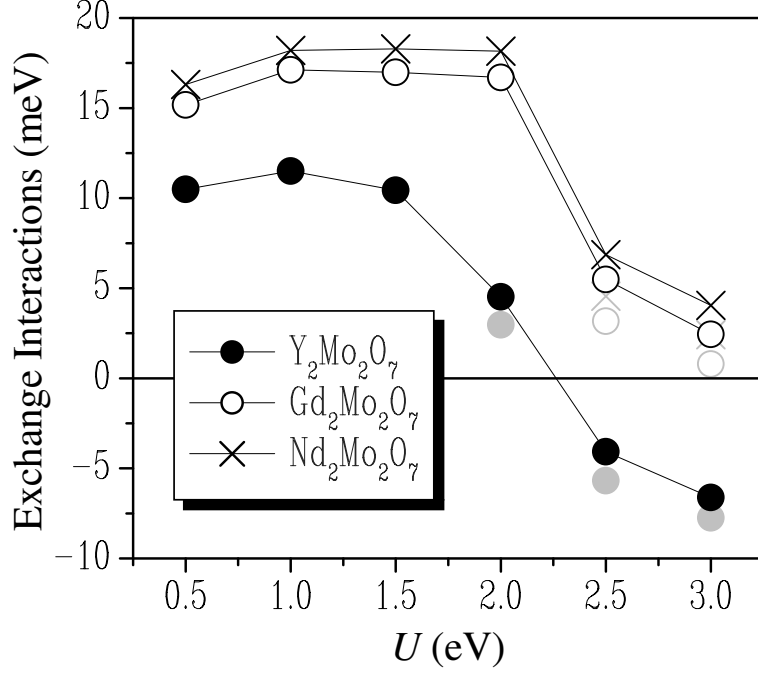


FIG. 10: Nearest-neighbor exchange interactions calculated in the ferromagnetic state. The orbital ordering realized for large  $U$  destroys the equivalence of some of the Mo-Mo bonds, that generally leads to the inequality  $J_{12}=J_{13}\neq J_{14}$ . Two such parameters,  $J_{12}$  and  $J_{14}$ , are shown by dark and light symbols, respectively.

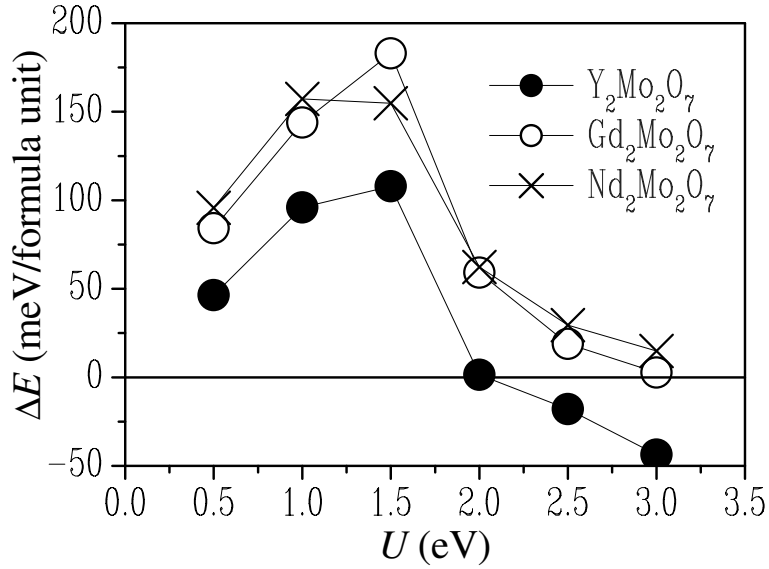


FIG. 11: Total energy of the antiferromagnetic state relative to the ferromagnetic state.

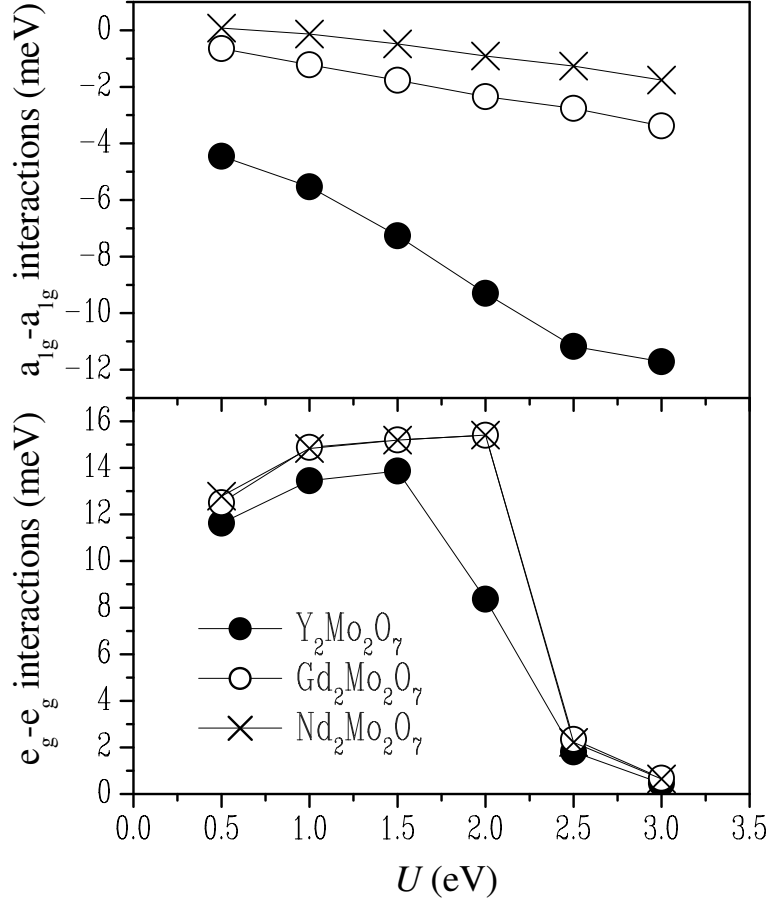


FIG. 12: Contributions of  $a_{1g}$  and  $e'_g$  orbitals (coming from the  $t_{2g}$  manifold in the local coordinate frame) to the exchange constant  $J_{14}$ .

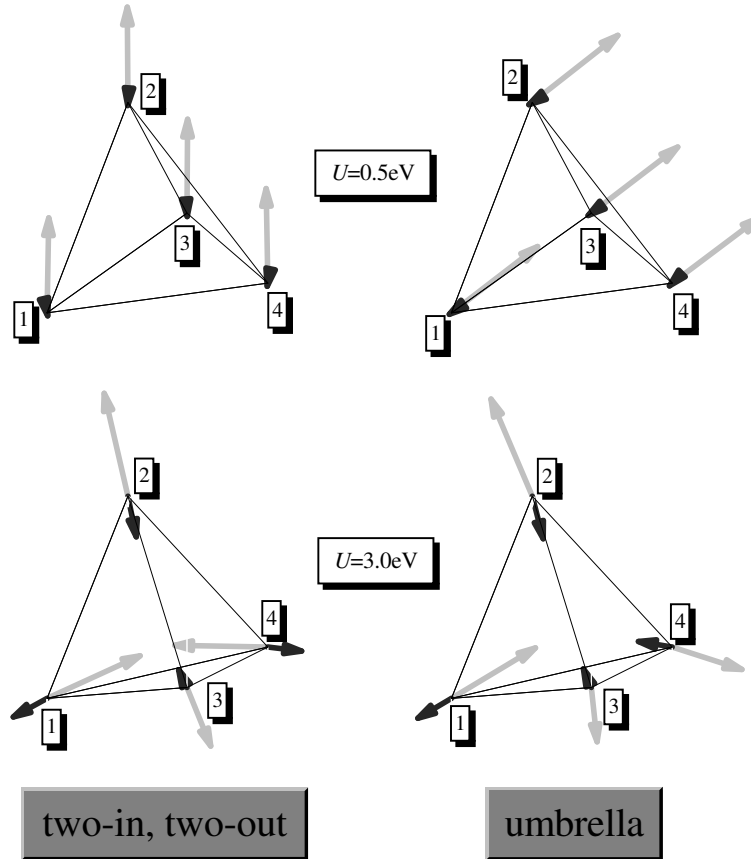


FIG. 13: Two magnetic structures realized in the case of the ferromagnetic coupling between nearest-neighbor Mo spins: "two-in, two-out" (left) and "umbrella" (right). The relative orientation and the magnitude of the spin (light vectors) and orbital (dark vectors) magnetic moments corresponds to  $\text{Gd}_2\text{Mo}_2\text{O}_7$  for two different values of the Coulomb interaction  $U$ .

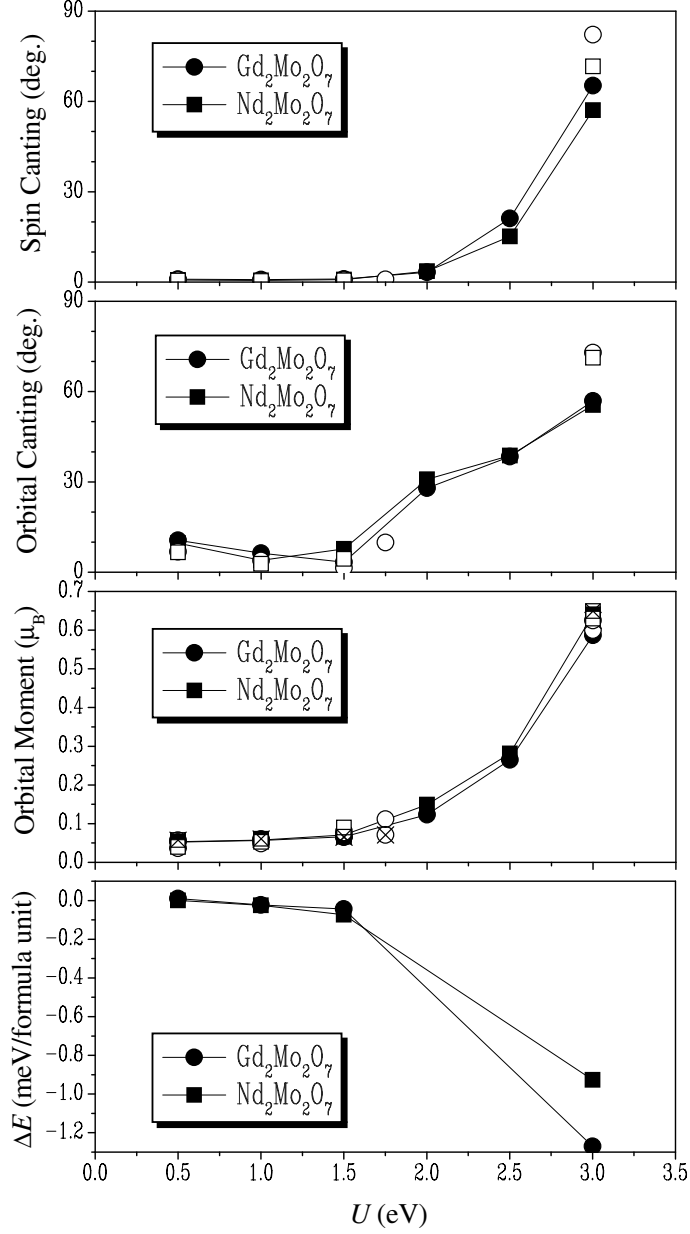


FIG. 14: The angles formed by the spin and orbital magnetic moments and either (0, 0, 1) ("two-in, two-out") or (1, 1, 1) ("umbrella") axes; the absolute value of the orbital moment; and the total energy of the "umbrella" structure relative to the "two-in, two-out" structure as a function of Coulomb  $U$ . Filled and open symbols correspond to the "two-in, two-out" and "umbrella" structure, respectively. In the case of "umbrella" structure, there are two different magnetic moments: the ones at the site 1 are shown by regular symbols,  $\circ$  and  $\square$ , and the ones at the site 2, 3 and 4 (forming the top of the "umbrella") are shown by crossed symbols. The spin magnetic moment is of the order of 1.5-1.6 $\mu_b$ , and weakly depends on  $U$ .

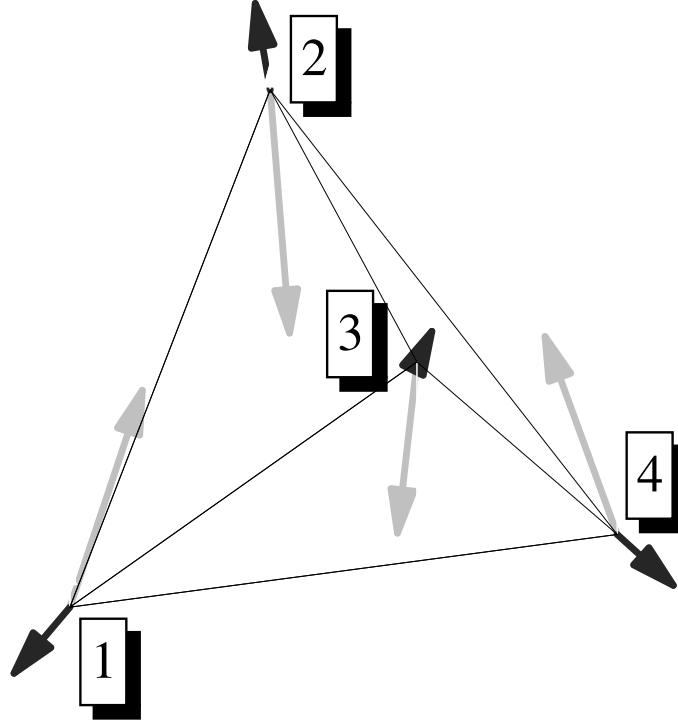


FIG. 15: Magnetic structure in the case of antiferromagnetic coupling between nearest-neighbor Mo spins. The relative orientation and the magnitude of the spin (light vectors) and orbital (dark vectors) magnetic moments corresponds to  $\text{Y}_2\text{Mo}_2\text{O}_7$  for  $U=3.0$  eV.

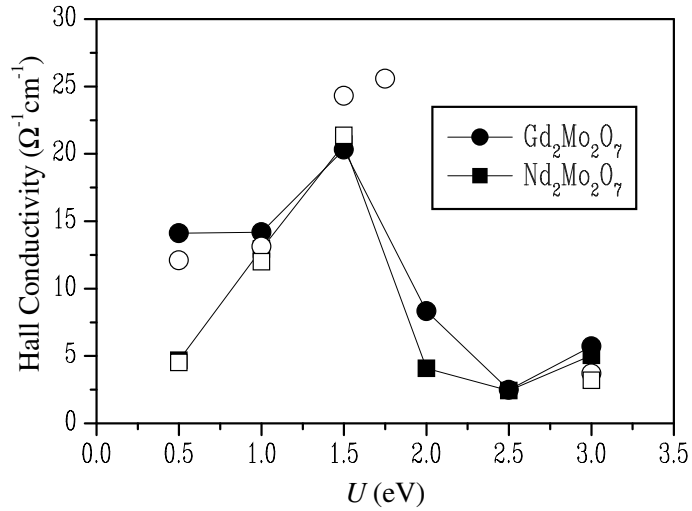


FIG. 16: Hall Conductivity in  $\text{Gd}_2\text{Mo}_2\text{O}_7$  and  $\text{Nd}_2\text{Mo}_2\text{O}_7$  as a function of Coulomb  $U$ . Filled and open symbols correspond to the "two-in, two-out" and "umbrella" structure, respectively.

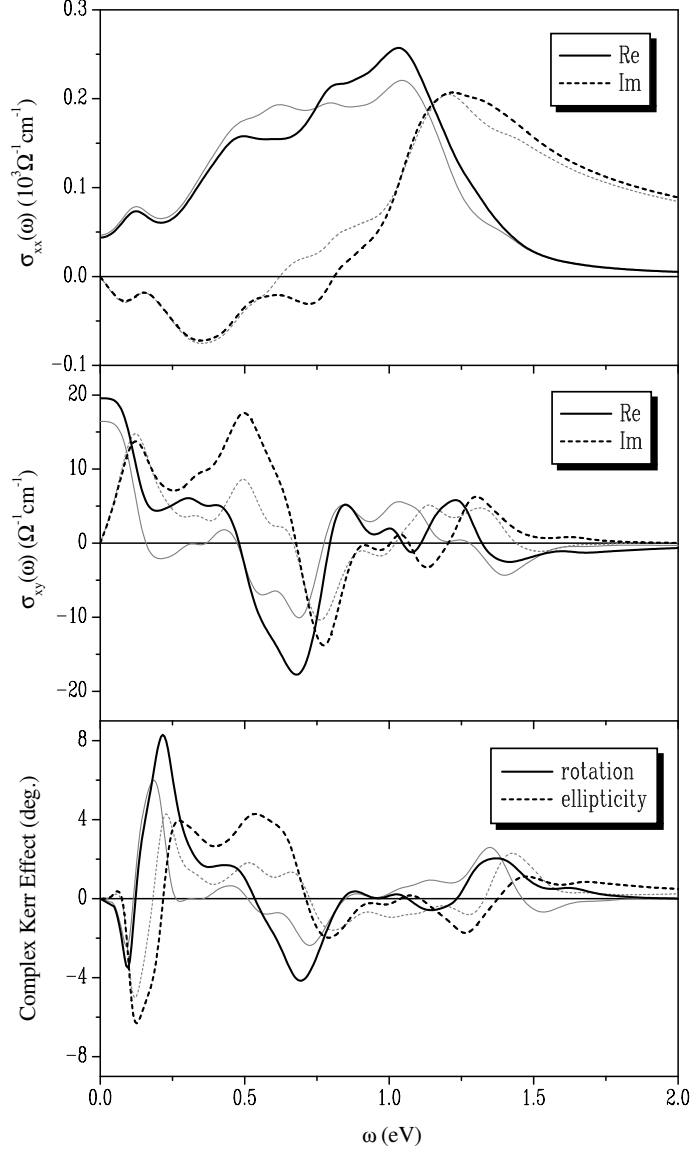


FIG. 17: Matrix elements of optical conductivity and the Complex Kerr effect for  $\text{Gd}_2\text{Mo}_2\text{O}_7$  corresponding to the "umbrella" ground state realized for  $U=1.5$  eV. Black lines show total spectra. Gray lines are obtained after excluding the  $a_{1g}$  orbitals from the wave functions (and roughly correspond to the partial contributions of the  $e'_g$  bands).